Aalto University
School of Chemical
Technology

School of Chemical Technology
Degree Programme of Materials Science and Engineering

Niklas Wester

TETRAHEDRAL AMORPHOUS CARBON – GRAPHENE HYBRID ELECTRODE FOR DETECTION OF DOPAMINE

Master's thesis for the degree of Master of Science in Technology submitted for inspection, Espoo, 19 August, 2015.

Supervisor **Professor Jari Koskinen**

Instructor **D.Sc. Vera Protopopova**

Author Niklas Wester

Title of thesis Tetrahedral Amorphous Carbon – Graphene Hybrid Electrode for Detection of Dopamine

Department Materials Science

Professorship Materials Processing **Code of professorship** MT-45

Thesis supervisor Prof. Jari Koskinen

Thesis advisor(s) / Thesis examiner(s) D.Sc. Vera Protopopova

Date 19.08.2015 **Number of pages** 90 **Language** English

Abstract

The real time in vivo detection of dopamine and other neurotransmitters in awake behaving animals is a long-standing goal. Carbon nanomaterials have emerged as promising candidates for electrochemical detection of dopamine. Diamond-like carbon films have wide water window, low capacitive background current and high chemical stability. By combining ultrathin tetrahedral amorphous carbon (ta-C) with Ti under layer the electron transfer properties can be enhanced without deterioration in the desired properties of ta-C. Such a bilayer thin films can also be modified with other carbon allotropes, such as graphene.

To the best knowledge of the author this reports for the first time a ta-C electrode modified with reduced graphene oxide (rGO) for electrochemical detection of dopamine. Ti/ta-C bilayer electrodes with varying ta-C top layer thickness were fabricated and optimized in terms of electron transfer properties. Both types of electrodes were subjected to cyclic voltammetry experiments, Raman spectroscopy, Fourier transform infrared spectroscopy (FT-IR), and scanning electron microscopy. The ta-C thickness was found to affect the electron transfer kinetics, while the dopamine detection limit of 5 µM remained unchanged. The electron transfer properties were found to improve with decreasing ta-C thickness and best performance was observed with 7 nm ta-C thickness. At a thickness below 7 nm the electron transfer properties start deteriorating due to excessive oxidation of the Ti/ta-C interface. The ta-C electrode showed poor selectivity towards dopamine. An order of magnitude improvement in sensitivity and a significant increase in selectivity towards dopamine was achieved. The rGO modified electrodes were able to detect 500 nM DA without any data treatment. Modification with rGO also resulted in significant improvement in electron transfer kinetics of dopamine. The amount of added rGO and the stacking of the graphene sheets were found to affect electron transfer in both inner and outer sphere systems. Finally oxidative treatments of the rGO resulted in increased current response and selectivity towards dopamine of all rGO electrodes, highlighting the role of oxygen containing functional groups in the electro-oxidation of both L-ascorbic acid and dopamine.

By combining the stability, good electron transfer properties, and the reasonably low capacitive currents of the Ti/ta-C bilayer electrode with the more electrochemically active rGO, an electrode with low detection limit and improved selectivity towards dopamine was achieved. This electrode also exhibited wide enough water window and sufficiently low capacitive background currents for electrochemical detection of dopamine.

Keywords Dopamine, graphene, ta-C, cyclic voltammetry

Tekijä Niklas Wester

Työn nimi Tetraedrinen amorfinen hiili – grafeeni hybridielektrodi dopamiinin havaitsemiseen

Laitos Materiaalitekniikka

Professuuri Materiaalien prosessointi **Professuurikoodi** MT-45

Työn valvoja Prof. Jari Koskinen

Työn ohjaaja(t)/Työn tarkastaja(t) TkT Vera Protopopova

Päivämäärä 19.08.2015 **Sivumäärä** 90 **Kieli** Englanti

Tiivistelmä

Dopamiinin ja muiden hermovälittäjäaineiden reaaliaikainen havaitseminen elävissä organismeissa on pitkäaikainen tavoite. Hiilinanomateriaalit ovat osoittautuneet lupaaviksi materiaaleiksi dopamiinin havaitsemiseen. Timantinkaltaisella hiilellä on laaja vesi-ikkuna, matala kapasitiivinen taustavirta ja se on kemiallisesti stabiili. Yhdistämällä ultraohut tetraedrinen amorfinen hiili (ta-C) titaanin kanssa saadaan aikaan kaksikerroksinen elektrodi, jonka elektroninsiirto-ominaisuuksia voidaan säätää muuttamalla ta-C – kalvon paksuutta. Tämän elektrodin pintaa voidaan myös modifioida muilla hiilen allotroopeilla, kuten grafeenilla.

Modifioimme ensimmäistä kertaa Ti/ta-C -elektrodeja grafeenilla dopamiinin havaitsemista varten. Ti/ta-C elektrodien elektroninsiirto-ominaisuudet optimoitiin ensin muuttamalla ta-C kerroksen paksuutta. Molemmat elektrodit karakterisoitiin syklisellä voltametrialla, Raman ja FT-IR spektroskopialla sekä pyyhkäisyelektronimikroskopialla. Elektroninsiirron havaittiin olevan riippuvainen ta-C:n paksuudesta, vaikka paksuudella ei ollut vaikutusta dopamiinin 5 µM havaitsemisrajaan. Elektroninsiirto kasvoi, kun ta-C:n paksuutta pienennettiin. Alle 4 nm paksuudella elektroninsiirto kuitenkin hidastui johtuen Ti -alikerroksen passivoitumisesta. Ti/ta-C elektrodi ei ollut selektiivinen, eivätkä askorbiinihapon ja dopamiinin hapetuspiikit olleet erotettavissa. Grafeenin avulla saavutettiin yhden kertaluokan aleneminen havaitsemisrajassa. Grafeeni-Ti/ta-C -elektrodilla saatiin 500 nM havaitsemisraja dopamiinille. Grafeeni myös nopeutti dopamiinin hapetus-pelkistysreaktion kinetiikkaa ja paransi selektiivisyyttä. Askorbiinihapon ja dopamiinin hapetuspiikit voitiin erottaa toisistaan. Lisäksi grafeenin määrän ja agglomeraattien mikrorakenteen havaittiin vaikuttavan elektroninsiirtoon sekä ulko- että sisäkehän hapetus-pelkistysreaktioissa. Lopuksi grafeenia hapetettiin väkevällä typpihapolla, minkä voitiin todeta kasvattavan dopamiinin virtavastetta sekä elektrodin selektiivisyyttä.

Yhdistämällä Ti/ta-C -elektrodin elektroninsiirto-ominaisuudet ja matala taustavirta sähkökemiallisesti aktiivisemman grafeenin kanssa saatiin aikaan selektiivinen elektrodi, jolla on tarpeeksi matala havaitsemisraja dopamiinin havaitsemiseen solujen ulkoisessa nesteessä aivoissa. Lisäksi tämän elektrodin vesi-ikkuna on riittävän suuri ja taustavirta tarpeeksi pieni dopamiinin sähkökemiallista havaitsemista varten.

Avainsanat Dopmiini, grafeeni, ta-C, syklinen voltametria

Acknowledgements

First of all I would like to thank Prof. Jari Koskinen and Prof. Tomi Laurila for granting me the opportunity to work in this project. Both my supervisor Prof. Jari Koskinen and Prof. Tomi Laurila showed interest in my work and gave me useful guidance and support.

I would also like to thank D.Sc. Vera Protopopova, M.Sc. Tommi Palomäki and M.Sc. Ajai Iyer for getting me started with this work and familiarizing me with the measurements. They also provided help and support for much of the measurements throughout the working process.

In addition I would like to thank all the other people who have contributed to this work in different ways. I would like to thank D.Sc. Vivek Singh, who synthesized the reduced graphene oxide used in this work, M.Sc. Ajai Iyer for helping me with the Raman Spectroscopy, and M.Sc. Anne Tanskanen for performing FT-IR measurements. I am also grateful to M.Sc. Sami Sainio who provided peer support and worked with me in developing the electrode contacting method and other practical issues with the electrochemical measurements. M.Sc. Ville Rontu also deserves thanks for helping me with the writing of the thesis.

Finally I would like to thank my family and my girlfriend Lotta Vuolamo for their love and support during the writing of this thesis.

Contents

1 Introduction

Dopamine (DA) is an extrasynaptic neurotransmitter that has an important role in cognitive, behavioral and motor functions as well as neuronal plasticity, learning, memory, attention span and the brain reward system [1–4]. Irregular dopamine concentrations, and especially total depletion of dopamine in the central nervous system, has been implicated in several illnesses, such as schizophrenia [2], Parkinson's disease, attention-deficit hyperactivity disorder (ADHD) and Tourette's syndrome. Dopamine also has a significant role in drug addiction, as it is involved in the brain reward system and all drugs affect the dopamine mediation process [2] [5] [6]. According to estimates as many as 27 % of the adult population in Europe are affected by mental and neurological disorders [7]. Despite the importance of dopamine and the involvement in these disorders, its precise role in them is as of yet not fully understood. [1–3]

The implication of dopamine in many crucial functions makes the ability to measure dopamine concentrations in real time an attractive prospect. The ability to measure dopamine levels in the brain with high sensitivity and selectivity, could likely contribute greatly to the understanding of the systems that dopamine is involved in. Two challenges persist in measuring the DA concentrations in the brain over meaningful periods of time. First the dopamine basal concentration in the brain extracellular fluid is low, on the order of 5–100 nM. Second high selectivity is required as interferents, such as ascorbic acid and uric acid are present in orders of magnitude greater concentrations. [3] At present the research focuses mainly on improving sensitivity, selectivity, and biocompatibility of the applied electrodes [2].

Over the past several years the electrochemical properties of both ta-C [8–10] and graphene [11–13] have been studied extensively. Diamond-like carbon (DLC) has been shown to have excellent chemical stability and biocompatibility, as well as low capacitive background current. Recently a Ti/tetrahedral amorphous carbon (ta-C) bilayer electrode with dopamine detection limit close to physiological concentrations was reported. [8] [10] This electrode is however not sufficiently selective towards DA in system containing the interferant Ascorbic Acid (AA) [14]. Owing to its electrochemical properties graphene has

been applied in electrochemical detection of dopamine to improve both sensitivity and selectivity towards dopamine [15–18].

The aim of this work is to fabricate Ti/ta-C bilayer electrodes with different thickness and study the effect of the ta-C thickness on the heterogeneous electron transfer properties as well as sensitivity and selectivity towards DA. Optimized Ti/ta-C electrodes will then be modified with different amounts of chemically reduced graphene oxide (rGO) to find out if the detection limit can be lowered to physiologically relevant levels and selectivity in the presence of AA improved. Cyclic voltammetry experiments will be carried out to evaluate the electrochemical performance of both types of electrodes.

2 Literature review

2.1 Neurotransmitters

Neurotransmitters are amino acids, amines, and peptides secreted by neurons that relay messages to target cells [3]. The neurons in the central nervous system are responsible for information integration and control [6]. Neurons have a cell body with a nucleus. They also have specialized processes for input and output, dendrites being involved in the former and axons in the latter [3]. The neurons are connected through synapses where axons form connections with cell bodies and dendrites of other neurons. These neuronal networks in the mammalian brain process a vast amount of information provided by the senses of the subject. Much of this signaling is mediated by neurotransmitters [6].

Neurotransmitters are stored in the synaptic vesicles in the axon end of a neuron. The release of neurotransmitters is usually followed by uptake by receptors on an adjacent neuron. The uptake is done by transporters, which are membrane bound proteins, and transport extracellular neurotransmitters back into the cell. The neurotransmitters that are not taken up by transporters readily diffuse out of the neuronal region and are subsequently metabolized. [1] The understanding of chemical neurotransmission events of the brain is not as well developed as the neuron doctrine and the understanding of the electrical processes in the brain. The development of a better understanding of the specific roles and functions of neurotransmitters has been impeded by the inability to study neurotransmissions in real time in awake, behaving animals. [3]

2.2 Dopamine

Dopamine (3,4-dihydroxyphenetylamine) is synthesized in dopaminergic neurons and stored in vesicles, from where it is released by electrical impulses [6]. It is an important neurotransmitter known to be an extrasynaptic messenger that functions via volume transmission, escaping the synaptic cleft and subsequently binding to receptors and transporters [4]. Figure 1 shows the dopaminergic neuron and the vesicles from which dopamine is released into the synapse.

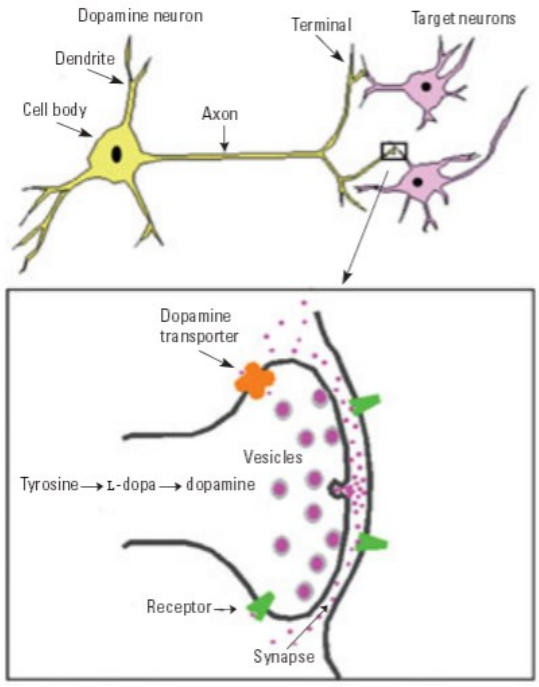

Figure 1. The dopaminergic neuron and the synapses. [6]

Dopamine is synthesized by decarboxylation of 3,4-dihydroxyphenylalanine (DOPA) and it is the precursor for adrenaline and noradrenaline. These neurotransmitter belong to the catecholamine family. Dopamine contains a catechol core, a benzene ring with two hydroxyl (OH) groups, and an amine (NH_2) group. [2]

In physiological conditions dopamine occurs in the form of an organic cation [2]. The catecholamine affects cognitive, motoral and behavioral functions. In addition it is of crucial importance in the attention span, learning, and memory. DA also affects the cardiovascular and renal system and plays a role in motivated behavior, such as perceiving rewards and pleasure. [1] [3] Low levels or depletion of dopamine is implicated as a major cause in several neurological diseases, such as schizophrenia, Parkinson's disease, and ADHD/ADD [2]. All drugs of abuse affect the dopaminergic pathway and therefore much of the study of addiction focuses on dopamine. [2] [5] [6] Despite the important role of dopamine in these conditions as well as in behavior and the brain reward system, the precise function is not fully understood. [2] [3]

The involvement of dopamine in many physiological, behavioral, and pathological functions makes the ability to study dopamine levels in vivo an important tool for further

development of the understanding of the specific role of dopamine. Real time information about neurotransmitter levels in awake behaving animals may likely contribute to improved disease diagnosis and treatment of neurological disorders.

2.3 Electrochemistry of neurotransmitters

Neurotransmitters are either electroactive or non-electroactive. Tyrosine derivatives dopamine, norepinephrine, and epinephrine belong to the former group and can therefore be detected by electrochemical means. Other electroactive neurotransmitters include catechol metabolites, such as 3,4-dihydroxyphenylacetic acid (DOPAC), homovanillic acid, 3-methoxytyramine, and 3,4-dihydroxyphenylalanine (L-DOPA) as well as neuroactive tryptophan derivatives 5-hydroxytryptamine (Serotonin), 5-hydroxyindolacetic acid, 5-hydroxyindoletryptophan and melatonin. In addition histamine and adenosine show electroactivity and can be detected by electrochemical means. [3] All electroactive neurotransmitters and other electroactive compounds are of interest for in vivo electrochemical detection as they all produce their own peaks, and can be difficult to differentiate from the analyte of interest. These other electroactive compounds include ascorbic acid, uric acid, nitric oxide, molecular oxygen, and hydrogen peroxide.

The group of non-electroactive neurotransmitters can further be divided into two groups, the first of which can be oxidized by enzymatic reactions and coupled with electrochemical detection. Amino acid transmitters, such as glutamate and γ-aminobutyric acid GABA, as well as acetylcholine and its precursor choline, belong to this group. Neuropeptides and some amino acids constitute the latter group, and can presently not be detected by electrochemical means. [3]

2.4 Techniques for measurement of neurotransmitters in the brain

The ability to directly measure the chemical communication between neurons in the brain is a long-standing goal. The most widely applied method is microdialysis, but spectroscopic techniques and in vivo voltammetry are also commonly applied. The techniques for detecting neurotransmitters can be divided into electrochemical and non-electrochemical. Microdialysis and spectroscopy are non-electrochemical methods, while common electrochemical methods include voltammetric and amperometric methods.

2.4.1 Non-electrochemical techniques

Microdialysis utilizes a perfusion pump within a dialysis membrane implanted in the brain. Small molecules can exchange across the membrane into the dialysate, which is removed for analysis. A typical flow rate of microdialysis experiments is 10 µL/min, restricting the practical sampling interval to 10 min. The long sampling interval ensures that sufficient dialysate can be extracted for handling and analysis. This sampling interval is ideal for monitoring the effects of pharmacological agents, as reaching the brain takes time and the effects may be long-lasting. This sampling interval is, however, not fast enough to determine the role of neurotransmitters in behavioral events. In addition the typical size of a microdialysis probe has a diameter in excess of 200 µm, which is large compared to the nerve terminals (~1 µm). This causes the brain tissue as far as 1 mm from the implantation site to be perturbed. [3] This can lead to considerable distortion of the extracellular neurotransmitter concentration [19]. Despite these shortcomings microdialysis is relatively easily applied in the study of various extracellular neurotransmitters. In addition the chemical resolution is excellent, as the dialysate can be analyzed by virtually any technique. Recent advances in microdialysis have reduced the sampling interval down to 1 min, and below in some experiments. [3] Even this sampling interval is insufficient, as DA transient duration is in the millisecond range.

Spectroscopic methods are non-invasive and have the ability to provide spatial resolution, giving maps of neuronal activity. The main spectroscopic methods are functional magnetic resonance imaging (fMRI) and positron emission tomography (PET). PET requires the use of positron emitting agents. They are usually activators or inhibitors of the receptors of the neurotransmitter of interest. Insights into brain regions involved in various behaviors can be gained through displacement of the endogenous ligand. Functional magnetic imaging (fMRI) utilizes hydrogen spins and is able to provide approximately 4 mm resolution in human subjects. The amount of oxygen in the hemoglobin alters the local magnetic field hence the change in hydrogen spins. The blood oxygen level can be used to indicate neuronal activity, but assigning the changes to specific neurotransmitters requires the use of pharmacological agents. [3]

2.4.2 Electrochemical techniques

Electrochemistry is a powerful tool for monitoring electroactive species in living organisms in real time. Electrochemical methods enable high time resolution, which allows for determination of the role of a specific neurotransmitter in the execution of behavioral tasks. [3] The electrodes employed need to show high selectivity and be sufficiently sensitive to be able to detect the neurotransmitter of interest in the physiological concentration range. [2] [3] The most commonly applied electrochemical means for detecting DA are constant-potential amperometry, chronoamperometry, differential pulse voltammetry and fast scan cyclic voltammetry. Cyclic voltammetry is discussed in greater detail in the chapter 2.5.

In constant-potential amperometry the working electrode is held at sufficiently large potential to oxidize or reduce the species of interest, and current is measured. The amount of species that undergo electron transfer is related to the measured current by Faraday's law. The sampling rate of this method can be in the kHz range, allowing for sub-millisecond time resolution. Another advantage is the instantaneous reaction of the compound of interest, upon contact with the electrode, making it independent of adsorption effects. Constant-potential amperometry is, however, non-selective, as all species that can be electrolyzed at the applied potential will undergo reaction. [3] [20] The selectivity is somewhat increased in chronoamperometry, in which the potential is instantaneously stepped from an initial potential at which no electrochemical reaction occurs. After the stepping of the potential to a value at, which the species of interest is electrolyzed, a current is observed. For a diffusion controlled reaction the current decays with the inverse of the square root as the current is proportional to the concentration of the electroactive species. After this step the potential is stepped back to the initial holding potential. At this point the initially oxidized species is reduced, given that the reaction is reversible. [3] [20] This feature gives limited selectivity. In the case of a binary solution with DA and AA for example, the DA can be reduced after oxidation, whereas the electrochemical reaction for AA is irreversible.

Differential pulse voltammetry (DPV) combines linear sweep voltammetry and square wave techniques. A square wave of small amplitude is applied with constant frequency on a linearly swept potential ramp. The current is measured shortly before and after the square

wave is applied. The difference in the obtained currents is subsequently plotted versus the linearly swept potential. [3] In this method the measured current is also proportional to the analyte concentration on the electrode surface. DPV can differentiate between several analytes as long as their oxidation potential differs by more than 100 mV [21]. This makes DPV more selective than amperometric techniques. In addition DPV is among the most sensitive techniques for the direct evaluation of analyte concentrations. [20] A drawback of DPV is the relatively poor time resolution, as the duration of a typical scan is around 30 s [3].

2.5 Cyclic voltammetry

2.5.1 Cyclic voltammetry measurements

Voltammetry is a powerful tool for simultaneous qualitative evaluation of electroactive species with good temporal and spatial resolution. Fast scan cyclic voltammetry (FSCV) is one of the most common electrochemical methods for researching the change of neurotransmitter concentrations in the brain. In cyclic voltammetry the potential at the working electrode is swept from an initial potential E_i to the switching potential E_λ. The potential is swept linearly and the most common adjustable parameter is the sweep rate or scan rate υ. The potential range is chosen in such a way that all desired redox reactions can occur. In aqueous electrolytes the potential range is, however, limited by the water window of the electrode, as potentials of the onset of hydrogen and oxygen evolution should not be exceeded. [20]

During the forward scan (increasing potential) anodic reactions give rise to an anodic current. When the oxidation potential of the analyte is reached, the analyte oxidizes leading to an anodic current. The current resulting from electron transfer between species and the electrode is proportional to the scan rate υ, the electrode area A and the amount of electrical charge consumed in the reaction nF, and gives the equation for the faradic current

$$i = nFA\upsilon \tag{1}$$

The electrochemical reaction leads to decreasing analyte concentration at the electrode, and mass transfer of new analyte to the electrode from the bulk solution. As the potential increases the reduced form of the analyte is completely depleted from the electrode surface,

causing the mass transfer of new analyte to the electrode to reach its maximum value. At this point maximum current of the anodic peak is reached. With increasing potential the analyte depletion zone widens, leading to a widening of the diffusion layer and consequently a decrease in mass transfer to the electrode. At this point a decrease in current can be observed. When the switching potential is reached the scan rate becomes negative and the reverse scan (decreasing potential) begins. During the reverse scan the oxidized species are reduced, given that the electrochemical reaction is reversible. A cathodic peak with similar shape is obtained. The complete cycle gives a so called cyclic voltammogram, in which current is commonly plotted as a function of applied potential. [20] [22] The cyclic voltammogram of a reversible analyte is showed in Figure 2.

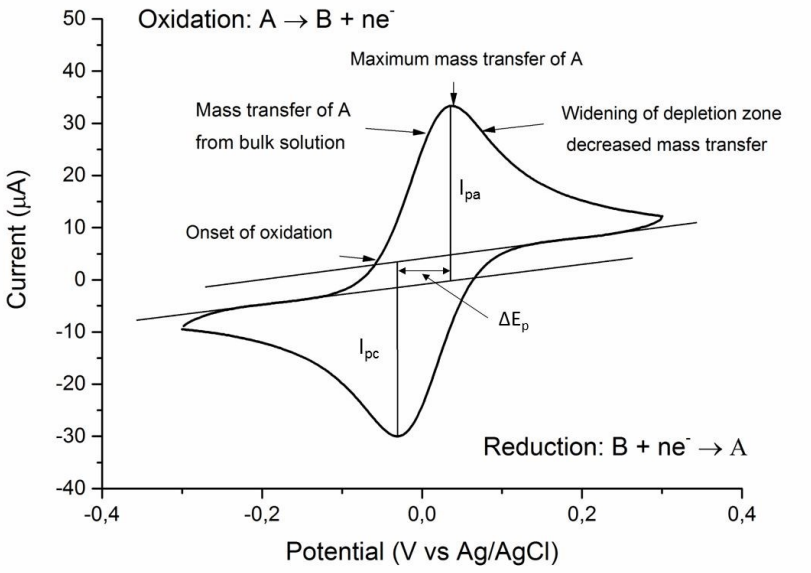

Figure 2. Cyclic voltammogram of a fully reversible outer sphere redox reaction.

The peak current ratio i_{pa}/i_{pc} and peak potential separation ΔE_p, obtained from the cyclic voltammogram provides information about the kinetics and reversibility of an electrochemical system. In a totally reversible or a Nernstian system all the oxidized species would reduce on the reverse scan. In such a case virtually all the oxidized species undergo reduction on the reverse scan and there is no deviation from unity in the peak current ratio i_{pa}/i_{pc}. In addition a Nernstian system has a peak separation ΔE_p between the anodic peak potential E_{pa} and the cathodic peak potential E_{pc} of $2.3RT/nF$ or 59/n mV at 25 °C, where n denotes the number of electrons transferred in the reaction. Completely

Nernstian systems are difficult to achieve at scan rates used in FSCV, as the electron transfer between the redox-active species and the electrode is often quite slow. [20] Achieving a Nernstian system is easier with slower scan rate. If the cycling rate is sufficiently increased, a point at which electron transfer starts to compete with the rate of potential change may be achieved. [23] By varying the cycling rate and observing the change in the peak potential separation, one can obtain information about the rate of heterogeneous electron transfer [20] [23].

Faster scan rates also lead to larger charging and faradic currents, with can lead to an increase in IR-drop as will be further discussed in chapter 2.5.2. By plotting the measured peak current as a function of scan rate one may obtain information about the faradic processes involved in the redox reaction. In diffusion controlled Nernstian systems the peak current is proportional to the square root of the scan rate $\nu^{1/2}$, whereas the current is directly proportional to ν in the case of an adsorbed species. [20]

2.5.2 Double layer capacitance and uncompensated resistance

The potential sweeping at a stationary, constant area electrode gives rise to a charging current [20]. A faradic current i_p causing a peak in the voltammogram involves transfer of electrons over the electrode-solution interface, leading to oxidation or reduction of a species. In the absence of faradic processes adsorption and desorption as well as changes in the structure of the electrode-solution interface may occur. Changes to the electrical double layer (EDL) typically happen when the potential at the electrode changes or solution composition changes. These processes where no electron transfer takes place are called nonfaradic processes, and they lead to a charging current i_c, which can be expressed as

$$|i_c| = AC_d\nu, \tag{2}$$

where A is the electrode area, C_d is the double layer capacitance, and ν is the cycling rate. [20] C_d is often measured for electrodes and reported as a measure of the charging current of the used electrode.

The electrochemical cell can be approximated as a RC-circuit. The resistance is the sum of solution resistance of the electrolyte R_s and the resistance of the capacitor C_d. [20] In

addition the electrode itself always has an electrical resistance, and ideally this value should be small compared to the solution resistance.

The solution resistance causes an ohmic drop iR_S to the potential applied to the working electrode. Good instrumentation and cell design can minimize the IR-drop, but it cannot be completely eliminated. This leads to the measured potential consisting of $E + iR_u$, instead of the actual potential of the working electrode. R_u is called the uncompensated resistance of a cell and it includes contributions from the solution resistance as well as the electrical resistance of the working electrode itself. An appreciable uncompensated resistance R_u compared to the accuracy of the measurement can cause non-linear sweeping of the potential at the working electrode. As the current increases with $\nu^{1/2}$, an increase in scan rate leads to larger shift in peak potential E_p. Large R_u values can therefore lead to similar effect as limitations in heterogeneous electron transfer kinetics, and cause the E_p to become a function of scan rate. In such a case the peak potential of an oxidation reaction is shifted to more positive potentials, and accordingly to more negative potentials for a reduction reaction. Increasing ν increases the peak potential shift. [20] In cyclic voltammetry experiments the uncompensated resistance in addition to the heterogeneous electron transfer rate becomes especially important as the scan rate is increased.

Modern instrumentation almost without exception has the ability to compensate the IR-drop. For example positive feedback IR-compensation is commonly applied. In this method an approximate value for the uncompensated resistance is measured, after which a potential of $E + iR_u$ is applied to the working electrode. Another common method is current interrupt IR-compensation. It can however be successfully used only for low scan rates of 10 mV/s or below.

The effect of the uncompensated resistance and double layer capacitance causes the electrochemical cell to work as an RC-circuit. In such a circuit the sum of the voltages across the resistor and the capacitor must be equal to the applied voltage, yielding

$$E = E_R + E_C = iR_S + \frac{q}{C_d} \tag{3}$$

Given that the current can be expressed as $i = dq/dt$ we obtain

$$\frac{dq}{dt} = \frac{-q}{R_S C_d} + \frac{E}{R_S} \tag{4}$$

In the case that the capacitor is initially uncharged (q = 0 at t = 0), and noting that E = νt for a liner sweep experiment such as CV, equation (3) can be expressed as

$$i = \nu C_d \left(1 - exp\left(-\frac{t}{R_S C_d}\right)\right) \tag{5}$$

In a potential step experiment the current exponentially decays with the time constant, $\tau = R_S C_d$. In CV the current increases from zero as the scan is started and attains a steady-state value νC_d. At the switching potential, E_λ, ν switches to –ν and the steady-state current changes to $-\nu C_d$. When the $R_S C_d$ value is small compared to ν, the steady-state current can be used to determine C_d as a function of E. More accurate double layer capacitance values can be obtained by electrochemical impedance spectroscopy (EIS). [20]

In a cyclic voltammetry experiment the peak current is related to the amount of species that undergo electrochemical oxidation or reduction. The charging current contributes to the measured peak current value, and must therefore be subtracted. If a peak baseline cannot be determined, Nicholson [23] has proposed the use of the following equation to determine the peak current ratio.

$$\frac{i_{pa}}{i_{pc}} = \frac{0.485(i_{pc})_0}{i_{pc}} + 0.086 \tag{6}$$

In long term in vivo measurements background subtraction can be problematic as background current drift has been observed on several types of electrodes. Usually the changes in background currents are large on the first cycle, but become smaller with continued cycling.

2.5.3 Electrochemical cells and electrodes

In cyclic voltammetry experiments one is usually interested only in the reactions that occur at the working electrode. To determine the potential at the working electrode, the cell also has a reference electrode, an electrode of known potential that approaches ideal nonpolarizability. Ideally the passage of current does not affect the potential of the reference electrode. The electrodes are separated by an electrolyte which works as an ionic

conductor. The electrolyte can be aqueous or non-aqueous and must have sufficiently low resistance. The electrode-electrolyte interfaces, the electrolyte and a potentiostat for applying and measuring potentials and currents constitute the electrochemical cell. [20]

If the IR-drop of the cell is small (1–2 mV), a two electrode cell can be used for CV measurements. Such is usually the case when an ultramicroelectrode (UME) is used. The currents that pass through UMEs are usually on the order of 1 nA, making even R_s values in the MΩ range acceptable. The small current also permits very high scan rates, on the order of 10^6 V/s, to be used [20]. The definitions for UMEs vary. Bard defined an UME as an electrode that has a critical dimension of 25 μm or less [20], whereas Compton gives the definition of smaller dimensions than the scale of the diffusion layer that forms during measurements [22]. Ultramicroelectrodes have a good signal-to-noise ratio, due to small charging currents and increased faradic currents due to high rates of mass transfer. The small charging currents also lead to small time-constants allowing for fast response time. For CV measurements with larger planar electrodes a three electrode cell is often utilized. The larger surface area leads to larger currents, which in some cases could lead to considerable IR-drop.

2.6 Measurement of dopamine by Cyclic Voltammetry

2.6.1 Electrochemical oxidation of dopamine

Dopamine as well as other catecholamine neurotransmitters are known to oxidize at +0.2 V, and can therefore be detected by electrochemical means with carbon and metal electrodes [3]. Several mechanisms for electrochemical oxidation of dopamine have been proposed by several groups, including EC [24], ECC [25], ECE [26], ECECEE [27]. The E denotes an electrochemical reaction, whereas the C describes a chemical reaction. The ECECEE mechanism proposed by Li et al. [27] is shown in Figure 3.

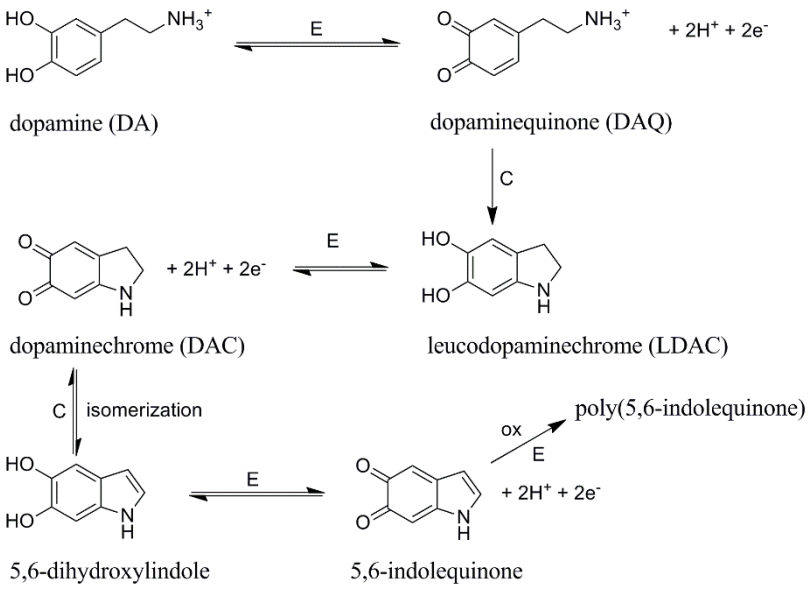

Figure 3. The dopamine oxidation pathway proposed by Li et al. [27]

The electrochemical detection of dopamine is related to the first electrochemical oxidation step, which includes transfer of two electrons and deprotonation of the catechol hydroxyl groups. The measured current response should be linearly dependent on the analyte concentration [2].

Despite a large number of publications on the electrochemistry of DA it is not entirely clear in what order the deprotonation and transfer of the two electrons takes place. It is also not clear if the electron transfer occurs as a one step process or if there is separate transfer of the two electrons. Corona-Avendano et al. [24], Wang et al. [15], Wen et al. [25],

Doménech et al. [28] have proposed that the electron transfer occurs in two consecutive one-electron transfer steps, resulting in the formation of an intermediate semiquinone.

In the first oxidation step dopamine is oxidized to dopamine ortho-quinone (DAQ). In CV some of the formed DAQ is reduced back to DA on the backward scan, depending on the reversibility of the reaction. The time before reduction potential is reached depends on the scan rate and potential window, and affects the time for which subsequent chemical or electrochemical reactions may occur. Further chemical reactions of DAQ lead to intramolecular cyclization [26] or further deprotonation of the amine group and the formation of leucodopaminechrome (LDAC). The deprotonation of DAQ is affected by solution pH, and does not occur below pH 5. [25] [27] In the reaction pathways that include a second electrochemical step, LDAC is oxidized to dopaminechrome (DAC) [26] [27]. This reaction however has slow kinetics, with a rate constant of $k = 0.1\ s^{-1}$, and can therefore be significantly inhibited by using fast-scan methods [2]. Li et al. [25] and Wen et al. [27] have reported that DAC can undergo polymerization reactions leading to the formation of a melanin-like polymer, and passivation of the electrode.

The electrochemical oxidation of dopamine is an inner-sphere reaction. Therefore it requires an adsorption step, and is strongly dependent on the electrode surface. DuVall and McCreery were able to severely inhibit the heterogenic electron transfer of catechols by organic monolayers of nitrophenyl, trifluoromethylphenyl, and methylene blue on a glassy carbon electrode. Chemisorbed or physisorbed monolayers of quinones, however, did not inhibit electron transfer, and were actually found to be catalytic towards DA oxidation. [29] The electron transfer through the adsorbed monolayer of quinones was attributed to self-catalysis [30]. The adsorption step prior to oxidation is proposed to be dependent on catechol adsorption [29] [30]. Contradictory results were reported by Bath et al. suggesting that the amine of DA is involved in the adsorption process [31]. Further evidence, showing that both the catechol and the primary amine functionality of DA can adsorb to active sites on glassy carbon (GC), was presented by Deinhammer et al. [32] They found that the nitrogen to carbon (N/C) ratio was significantly lower on the CG electrode after cycling in DA solution as compared to cycling in amine containing species, without the catechol functionality. Addition of catechol also leads to a large decrease in the surface N/C value

when cycling in N-acetyletylenediamine, which gives high N/C values in the absence of catechol. These immobilized DA molecules were shown to be electrochemically active, and peaks attributed to DA oxidation were observed. [32]

2.6.2 Special considerations for in vivo measurements

The real time in vivo detection of DA is challenging, due to various surface processes inherent to biological systems. For this reason it is important to understand both the analytical properties of the sensor material and the characteristics of the biological system. [6] Cyclic voltammetry provides good temporal, chemical and spatial resolution. Good temporal resolution however required the use of fast scan rates in excess of 300 V/s. The use of this scan rate results in cycles lasting only milliseconds, and allows for subsecond detection of neurotransmitters. [4] At these scan rates it is necessary to use microelectrodes to limit the effect of uncompensated resistance of the electrode. With microelectrodes the 2-electrode setup can also often be used without problems. [3] [20] The use of microelectrodes also limits the perturbation of the brain tissues. [3] Slow electron transfer kinetics may, however, cause shifts in redox peak potentials at fast scan rates. This may significantly reduce the selectivity of the sensor, as the shifts may cause peak overlap in multi-analyte systems. [4]

Despite the good temporal resolution of cyclic voltammetry measurements most electrodes show a delayed response to changes in DA concentration. [31] For this reason the understanding of the kinetics is important for correct interpretation of transient release and uptake of DA in in vivo measurements. Nicholson showed that the diffusion in the extracellular space is different from diffusion in solution as dilution is not as great as in bulk solution. The extracellular fluid accounts for a volume fraction of approximately 20% and the presence of neurons, glia, blood vessels and other cells also causes the diffusion path to be tortuous, slowing the effective diffusion rate. As a result diffusion rates approximately a third of in vitro bulk solution diffusion rates are expected in the brain [33]. Moreover DA transients only last a few milliseconds, due the fast uptake of DA by transporters that remove DA from the extracellular fluid. The diffusion distance of DA in extracellular fluid is therefore limited to only a few micrometers. [4] This makes fast response as well as placement of the electrode critical for in vivo detection of DA.

2.6.3 Interferents in measuring dopamine

Ascorbic acid (AA) and uric acid (UA) are considered the main interferents in electrochemical detection of DA. They are electrochemically oxidized at close to the same potential as DA, and are therefore difficult to distinguish with electrochemical methods. These main interfering molecules may be present in orders of magnitude greater concentrations. The AA concentration in the brain is on the order of 0.5 mM, while the basal concentration of DA is in the range of 5–100 nM. [4] Other important interferents are the other catecholamine neurotransmitters adrenaline and noradrenaline as well as DA metabolites, such as dihydroxyphenylacetic acid (DOPAC), homovanillic acid, 3-methoxytyramine and 3,4-dihydroxyphenylalanine (L-DOPA). In addition the tryptophan derivatives 5-hydroxytryptamine and its metabolites are electroactive and oxidize around +0.35 V. [3] Table 1 shows the interferents relevant to in vivo electrochemical detection of DA and their concentrations in the brain. It should be noted that the concentrations of these biomolecules depend strongly on the brain region and also on the method of analysis.

Table 1. Interferents relevant to electrochemical detection of DA.

Interferent	Oxidation Potential vs Ag/AgCl (V)	Concentration in the brain	References
Dopamine (DA)	0.2	0.05-0.10 µM 9–11000 pmol/g	[3], [34]
Ascorbic acid (AA)	0.2	220–510 µM	[35], [3]
Uric acid (UA)	0.3	60 nmol/g	[36] , [37]
Serotonin (HT-5)	0.35	0.1–2 nmol/g	[3], [38]
DOPAC	0.1	9–5800 pmol/g	[34]
Noradrenaline	0.2	54–340 pmol/g	[3], [34]
Adrenaline	0.2	0.2–280 ng/g	[3], [39]

AA is a powerful reducing agent, with a redox potential of 0.05 V at 30 °C and pH 7.4 [40]. In practice the oxidation potential at most carbon electrodes is, however, approximately the same as for DA, with a value around 0.2 V. Emerging carbon materials, such as carbon nanotubes [14], carbon nanofibers [41] and graphene [15–18] have been reported to be able to oxidize AA at potentials closer to the thermodynamically expected value. Oxidative chemical surface treatments of CNTs have been reported to reduce the oxidation potential further to values of –0.1 V vs. Ag/AgCl [14]. Under physiological conditions AA is readily reversibly oxidized to dehydroascorbic acid, which may further be irreversibly hydrolyzed to diketogulonic acid [40]. The reaction pathway for the electrochemical oxidation of AA is shown in Figure 4.

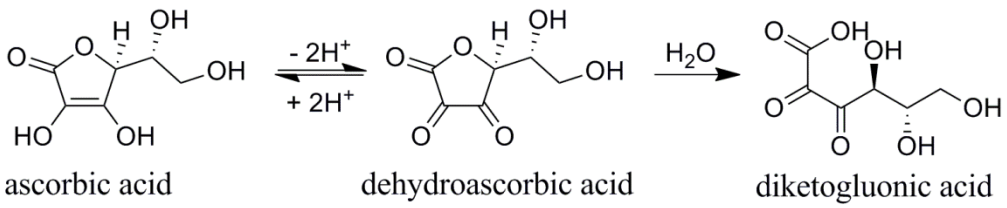

Figure 4. The reaction pathway for electrochemical oxidation of ascorbic acid. [42]

Ruiz et al. [42] showed that the two electron transfer electrochemical oxidation of AA is followed by rapid chemical reaction with water to form a stable hydrate. This causes the electrochemical redox reaction to be irreversible and the reduction rate to be controlled by the chemical step preceding the electrochemical reaction.

The levels of AA in the brain are in excess of 10 times that of serum concentration. L-ascorbic acid is not able to cross the blood-brain barrier, while dehydroascorbic acid is readily transported into the brain by glucose transporters. In the brain the dehydroascorbic acid is reduced. The reduction mechanism is unknown, but is believed to be related to glutathione and/or glutathione-dependent reductases. [43] As glutathione is known to be present at relatively high concentration in the extracellular fluid, reactions between glutathione and oxidized AA on the electrode surface cannot be ruled out. This may be a competing reaction with glutathione addition. The AA levels are stable compared to DA, but changes in AA concentrations are known to occur within seconds of physical stimulation and as an influence of administration of certain drugs [40].

Like ascorbic acid, uric acid is also a reductant present in the extracellular fluid working as a free radical scavenger [36]. UA has been shown to strongly adsorb to carbon and platinum electrodes, and oxidation starts at a potential of 0.3V. The redox reaction of UA is quasireversible, two electron transfer and the adsorption of UA was found to compete with the oxidation of AA, as the adsorbed UA to some extent inhibits the electron transfer of AA. [37] The electrochemical oxidation involves transfer of two electrons and a proton and results in the formation of an unstable diimine intermediate. The diimine can subsequently be hydrolyzed causing molecule rearrangement and loss of CO_2. [36]

In addition to the interferents presented above, sulfhydryl adducts of catechols have been found at around 0.1 to 1 % of DA concentration in the CNS [34]. Tse at al. [26] showed that the glutathione-dopamine adducts and DA do not differ enough to be distinguished by cyclic voltammetry. In addition the kinetics of the nucleophilic addition is fast and DAQ formed as a result of electrochemical oxidation of DA may lead to increase in these adducts. Such reactions may likely cause changes to the reaction pathway of DA. In addition a pH change can also cause interference in FSCV in vivo measurements. Changes in pH can induce changes in background currents and change the oxidation potential of catechols. [3]

[44] Several studies have shown that pH changes occur in the brain extracellular fluid and that these changes are related to dopaminergic activity [45] [46].

2.6.4 Electrode passivation

In addition to good selectivity towards DA, the successful in vivo measurements over meaningful time periods, requires the deleterious effect of electrode passivation to be overcome. It should be noted here that the measuring environment is a complex system of several co-existing compounds, and that this system is as of yet not fully understood.

In cyclic voltammetry experiments with DA the oxidation products of DA tend to react further to form passivating polymer films [27]. This phenomenon is also commonly referred to as electrode fouling. At high concentrations DA is known for its remarkable ability to spontaneously coat a wide range of organic and inorganic materials, including noble metals, oxides, polymers, semiconductors and ceramics, at mildly alkaline pH [47]. The passivation of the electrodes in DA detection is usually attributed to further reactions of the oxidation products of dopamine, mainly dopaminequinone (DAQ), which tends to react chemically to form aminochrome [2] [26]. Li et al. [27] found intramolecular cyclization to occur in DA solutions at concentrations above 200 μM and above solution pH of 3.86. Early work by Tse et al. [26] however showed that in the presence of AA the generated oxidized DA species DAQ are re-reduced by the AA. The rate of this re-reduction was found to be sufficiently fast to make the formation of aminochrome unlikely. They also determined the rates of nucleophilic addition of DAQ to other nucleophiles present in the extracellular fluid. The rates of addition to most amino acids were found to be relatively slow, slower in fact than the kinetics of the intramolecular cyclization. The addition to sulfhydryl compounds, such as glutathione (GSH) and cysteine, however has several orders of magnitude faster kinetics than the re-reduction process. Glutathione addition has sufficiently fast kinetics to occur when present in equimolar concentrations with AA. This concentration ratio has been found to represent the whole brain levels of small animals. [26]

Fornstedt et al. [34] found adducts of DOPA, DOPAC, and DA in the brains of several adult mammals, including human. The presence of these compounds was attributed to quinones, resulting from autoxidation of catechols, reacting with glutathione. Owing to the

fast kinetics of the addition reaction it is likely that the electrochemical oxidation of DA could lead to the formation of such adducts on the electrodes surface. Oxidized catechols are further known to react readily with sulfhydryl groups of proteins, causing protein inactivation. In addition to direct addition to the protein, protein and glutathione radicals can be produced resulting in protein cross-linking and glutathione dimer formation. Compounds containing catechol moieties, including L-DOPA, DA, and α-metyl-DOPA, can cross-link proteins. This reaction is accelerated by inducing oxidation (electrochemical or chemical), indicating that these oxidized catechol functionalities are responsible for cross-linking. The effects of these reactions on electrode fouling are unknown, but the much faster kinetics of the above competing reactions compared to intramolecular cyclization, makes extensive intramolecular cyclization of DAQ unlikely. The role of these sulfhydryl adducts, and their derivatives, in the passivation of electrodes in the extracellular fluid remains unclear. Moreover, electrode fouling is also commonly caused by adsorption of non-electroactive species, such as lipids, peptides, and high molecular weight proteins.

It is clear that the extracellular fluid is a complex environment that is not yet fully understood. Further research is needed to elucidate the mechanisms of electrode fouling. Today electrode passivation is mostly researched in greatly simplified systems that may serve as poor analogues for the environment and the chemistry of extracellular fluid. While these studies provide valuable contributions to the understanding of the chemistry and electrochemistry of these analytes, they are extensively simplified systems. Future work should focus on reactions which may occur between the oxidized forms of DA and reducing agents present in the extracellular fluid, as well as other biofouling mechanisms.

2.7 Properties of carbon electrodes

The electrochemical properties of carbon electrodes are often superior to noble metals in electrochemical measurement of biomolecules. Additional advantages include low cost, wide potential window, relatively inert electrochemistry and electrocatalytic activity for a wide range of redox reactions. [48] Carbon materials are also generally more biofouling resistant than metal electrodes [3]. They are, however, prone to reactions with oxygen and water. For this reason the surface of carbon electrodes always contain oxygen containing functional groups. The oxygen containing functional groups affect the adsorption

processes, electron transfer kinetics and water window among other things. To control the electrode surface chemistry surface preparation processes are commonly undertaken. These processes can be physical or chemical and involve polishing, cleaning, as well as vacuum and heat treatments. [48]

The electronic properties affect the electrochemical performance of electrodes [48]. The electron transfer in an electrochemical redox reaction involves quantum mechanical tunneling. The tunneling rate falls after distances of 1–2 nm are exceeded, as it requires overlap of the quantum mechanical wave functions. [22] The chemical species undergoing electrochemical redox reactions must be within 1–2 nm of the electrode surface. The electrical conductivity and density of states (DOS) of carbon materials varies greatly. Depending on the bonding configuration, the carbon material can be an electrical insulator or a conductor.

The conventional carbon electrodes are sp^2 hybridized graphitic electrodes, such as glassy carbon (GC) and highly oriented pyrolytic graphite (HOPG). More advanced graphite electrodes include edge plane pyrolytic graphite (EPPG) that has an edge with exposed individual graphitic planes, much like in graphene. These electrodes are still widely used both in research and industrial applications. [48] Electrodes fabricated from advanced carbon nanomaterials include carbon nanotubes (CNT), carbon nanofibers (CNF), carbon fibers (CF), boron doped diamond (BDD) and graphene. The different carbon electrodes are described in greater detail in chapter 2.8.

2.8 Carbon electrodes for electrochemical measurement

A wide array of carbon materials are employed in electrochemical measurements. Carbon electrodes are made from bulk material, synthesized nanoparticles and micro fabricated thin films. In this chapter these most common carbon electrodes are briefly presented. More focus is given to ta-C and graphene like materials, as these will be used as electrode materials in this work.

2.8.1 Graphite

Graphite consists of crystallites of parallel stacked two-dimensional graphene sheets. These graphitic electrodes are virtually fully sp^2 hybridized and have good conductivity. The electrical properties of graphite materials depend on the size of the crystallites [48]. The size and orientation of the crystallites vary depending on the method of synthesis. The size is often given as the in-plane size L_a and the size perpendicular to the planes L_c. Natural single crystal graphite and highly oriented pyrolytic graphite (HOPG) have large crystallites with L_a and L_c values exceeding 1µm. Natural polycrystalline graphite has significantly smaller L_a and L_c values of 10–100 nm. [48] The inorganic impurities, such as ash, in natural graphite, however, limits its use in electrochemistry.

HOPG is produced by decomposition of gaseous carbon precursors and subsequent high temperature high pressure pressing. Glassy carbon (GC) is an important electrode material. It is produced by heating polymers, often polyacrylonitrile, to 1000–3000 °C. At these temperatures the C–C bonds are not broken, which results in crystallites with L_a and L_c values of 30–70 Å. The interplanar spacing of approximately 3.6 Å is also larger than for HOPG. In contrast to HOPG the microstructure of GC consist of randomly intertwined graphitic planes. By mechanical cleaving of HOPG electrodes with majority of edge planes (EPPG) or basal planes (BPPG) can be fabricated. [48] These specially prepared electrodes have been used to research the electrochemical properties of edge plane and basal plane sites. The electrochemical oxidation of DA and AA on GC, EPPG and BPPG electrodes have been studied extensively [12] [49].

2.8.2 Carbon fiber

Carbon fiber (CF) electrodes have been used extensively in experimental work in neuroscience, where a small “footprint” is required [2] [48]. The diameter of CFs ranges from 5 to 50 µm, and can therefore easily the used to fabricate microelectrodes. In 1979 Ponchon et al. [50] first used a CF electrode for in vivo detection of catecholamine neurotransmitters. Since then a vast amount of in vivo measurements of DA with CF electrodes have been carried out. Today CF electrochemical sensors are still commonly used for in vivo measurements. [2] [51]

The general method of synthesis is CVD with small hydrocarbons as precursors. The crystallite orientation and order of CFs varies with the intended application. The three main types of CFs are radial, onion and randomly oriented fibers. In radial fibers the graphene planes radiate out from the center of the fiber, whereas the morphology of onion fibers is similar to that of CNTs. [48] The electrochemical performance of CFs in electrochemical detection of DA is well documented and has been found to be relatively unsusceptible to fouling by oxidized DA species. The sensitivity and selectivity of CFs has been enhanced by pretreatments and modification with CNTs, noble metals and conductive polymers. [2]

2.8.3 Diamond

Diamond is a fully sp^3 hybridized crystalline carbon material. The bonding configuration results in high hardness and makes it an electrical insulator, and therefore not interesting for electrochemical applications. The electrical conductivity can, however, be controlled by boron or nitrogen doping. Diamond has much greater chemical stability compared to sp^2 hybridized carbon materials. The excellent stability of diamond, enables the use of electrodes without pre-treatment, even after long storing at ambient conditions. [48]

The electrochemical properties of diamond have been studied extensively. The most common diamond electrode is the microcrystalline boron doped diamond electrode synthesized by chemical vapor deposition. [52] [53] The use of large single crystal BDD [54], nanocrystalline [55], and ultrananocrystalline diamond [56] electrodes have also been reported. The wide water window, small capacitive background currents and biocompatibility make BDD an interesting material for electrochemical applications. The main drawback with BDD and other diamond thin films is the high deposition temperatures, which leads to incompatibility with integrated circuit processing. [63]

The surface of diamond thin films can be functionalized by various treatments. It has been shown that extensive anodic tretments of BDD lead to oxidation of the carbon, and formation of oxygen containg groups. Anodized BDD shows significantly slower heterogenous electron transfer rates with AA compared to H-terminated BDD. [2] [48] Such a treatment is, however, expected to increase the occurrence of surface carbonyls, which have been shown to catalyze DA oxidation [30].

2.8.4 Diamond-like carbon

Diamond-like carbon (DLC) is a versatile amorphous carbon material with a large number of industrial applications. The properties of DLC are diamond like, but show a large range of variation due to sp^3/sp^2 ratio, and possible dopants and impurities. DLC thin films are commonly deposited by physical vapor deposition (PVD) and chemical vapor deposition (CVD). In this work DLC with high sp^3 content, reaching values up to 80 %, is employed. This DLC is called tetrahedral amorphous carbon, also known as ta-C and is usually deposited by PVD, but also CVD. [57] [58] The synthesis of ta-C is covered in greater detail in chapter 2.9.1. The ta-C deposited by CVD contains hydrogen from the hydrocarbon precursor. Figure 5 shows the ternary phase diagram of amorphous carbon-hydrogen alloys.

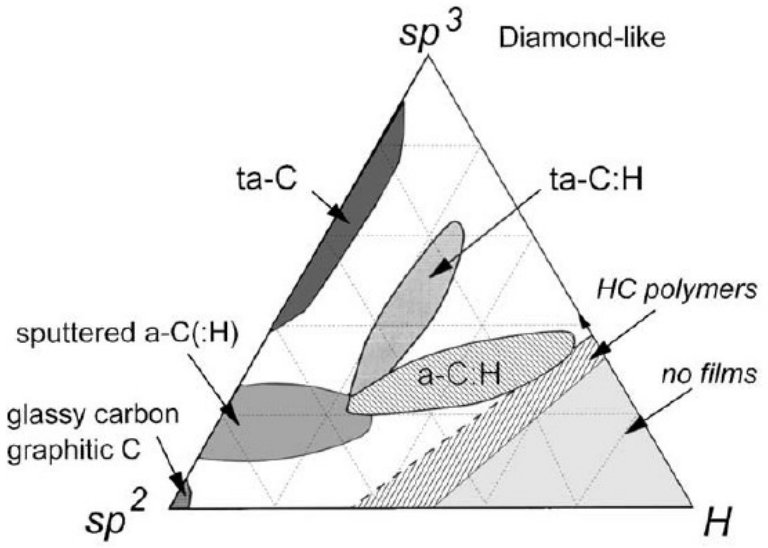

Figure 5. The ternary phase diagram of amorphous carbon-hydrogen alloys. [57]

Tetrahedral amorphous carbon has excellent mechanical properties, is highly corrosion resistant, and fully integrateable with current CMOS technology [57]. In addition DLC films are generally considered to be biocompatible [59] [60]. These properties are sought after in electrodes for electrochemical detection of biomolecules. Undoped ta-C is a p-type material with the Fermi level just below mid-gap. It can however be made a moderate electrical conductor by doping with nitrogen. [8] [57] The surface interface layer of the ta-

C has a significantly higher sp^2 character compared to bulk ta-C. The interface layer seems to be of relatively constant thickness, and for this reason an increase in total sp^2 hybridized carbon atoms can be observed as the thickness decreases. [61–63] This causes the possible coexistence of separate surface and bulk band gaps. The electric properties also cause ta-C to have low double layer capacitance when applied as an electrode material.

With outer sphere systems facile electron transfer can be achieved, and close to Nernstian systems have been reported at relatively fast scan rates in CV experiments. Several groups have reported such systems with nitrogen doped ta-C. Laurila et al. [8] recently achieved quasireversible electron transfer with a Ti/ta-C bilayer electrode. Benlahsen et al. [64] showed that cathodic pre-treatment in 0.5 M H_2SO_4 of magnetron sputtered a-C:N improved electron transfer in the $[Fe(CN)_6]^{3-/4-}$ system. They attributed the increase in electron transfer to the decrease of superficial nitrogen atoms involved in C–N sp^3 bond. Ultrathin undoped ta-C films have also been used for electrochemical detection of DA. [8] [10]

2.8.5 Graphene

Graphene is a two dimensional sheet of sp^2 bonded carbon atoms in a hexagonal configuration. This bonding configuration leads to properties, such as high surface area (2630 m^2/g), a tunable bandgap, high mechanical strength, high elasticity, as well as high electrical and thermal conductivity. [11] Unlike carbon nanotubes, graphene does not contain metallic impurities as an inherent property of the fabrication process. The absence of metallic impurities combined with low cost, high electrical conductivity and large surface area makes graphene a promising material for electrochemical sensing.

The good electrochemical properties of graphene are attributed to the edge-plane sites and defects in the basal planes [11]. The edge planes of graphene sheets in HOPG electrodes have an electron transfer rate of constant (k) of ~0.01 cm/s while the basal planes are electrochemically inert, with a k value of 10^{-9}. Brownson et al. [13] utilized density-functional theory (DFT) calculations to show that electron density of both highest-occupied molecular orbitals (HOMO) and lowest-unoccupied molecular orbitals (LUMO) is concentrated around the edge of the graphene sheets. It was also found that the probability that the electrons are concentrated around the edges increases with increasing size of the

graphene sheet. The density distribution of electrons in HOMO and LUMO orbitals for a 2x2, 3x3 and 4x4 is shown in Figure 6.

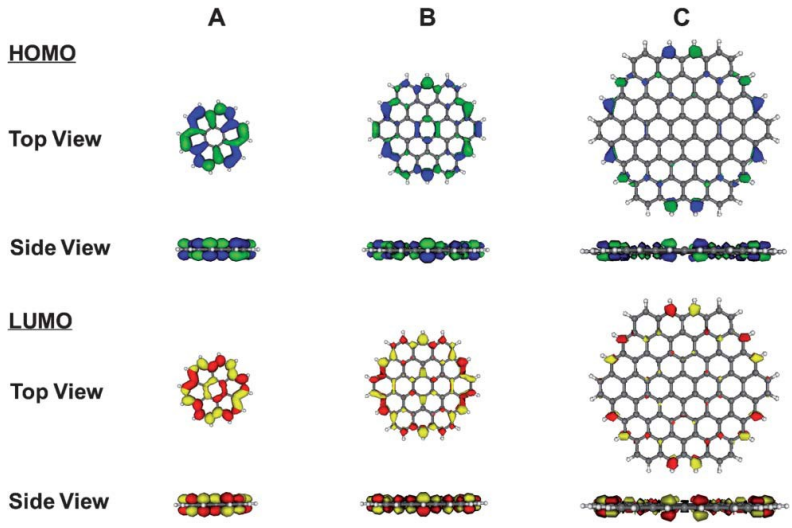

Figure 6. Electron density distribution in HOMO and LUMO orbitals for A) 2x2 sheet B) 3x3 sheet and C) 4x4 sheet. [13]

Even though graphene is regarded as being an excellent material for electrochemical electrodes, some groups have questioned this widely held opinion. Brownson et al. [13] conducted extensive studies with pristine monolayer graphene, and found that exposed basal planes inhibit the electron transfer of the underlying material. These studies were conducted by modifying bulk graphite electrodes. Li et al. [65], however, showed that the rates of electron transfer at individual monolayer graphene sheet microelectrodes show electron transfer rates of more than 10 times higher than for basal plane bulk graphite. They found electron transfer rate constants of ~0.5 cm/s and 0.042 for mechanically cleaved and CVD graphene, respectively. It should, however, be noted here that the electrochemical performance of graphene modified macroscale electrodes depend on the quality, morphology and the stacking of the graphene. These properties are strongly fabrication method dependent and such characteristics are discussed in greater detail in chapter 2.9.2.

Graphene, as all carbon materials, always contains some oxygen containing functional groups. The amount of oxygen can be changed by reduction and oxidation processes, but can never fully be eliminated at ambient conditions. [48] The oxygen containing groups have been found to facilitate catechol adsorption, and may therefore increase the sensitivity towards DA [29].

2.8.6 Carbon nanotubes and carbon nanofibers

Since the discovery of CNTs in 1991 they have generated interest due to their field emission and electronic transfer properties, high mechanical strength and chemical properties [66]. Carbon nanotubes are generally divided into single-walled carbon nanotubes (SWCNT) and multi-walled (MWCNT). SWCNTs consist of one rolled up graphene sheet capped by hemispherical ends. A typical diameter and surface area of a SWCNT is approximately 1 nm and 400–900 $m^2 g^{-1}$, respectively. MWCNTs have several layers, with a layer spacing of 0.3–0.4 nm and typical diameter and surface area of 2–100 nm and 200–400 $m^2 g^{-1}$, respectively. [66] [67] Methods of synthesis include arc discharge, laser furnace and CVD [66].

Large diameter MWCNTs are also called carbon nanofibers (CNF) [41] [68]. Another distinction of carbon nanofibers is that they have a very thin or no hollow cavity. They can have diameters up to 500 nm and surface areas in the range of 10–200 $m^2 g^{-1}$. The graphene planes in CNFs can be aligned parallel or perpendicular to their axis. CNFs can also have mixed orientations and such fibers are said to have "Herringbone" structure, and exhibit intermediate properties between ribbon and platelet CNFs. [67]

Metallic nanoparticles (typically Fe, Co, Mo and Ni) are used as catalysts in synthesis of CNTs and CNFs [69]. These metallic impurities in many cases dominate electrochemical systems even below 100 ppm levels [11]. Pumera et al. [11] concluded that the reason for fast heteroelectron transfer in carbon nanotubes is caused by defects. These defects have been found to be more abundant in MWCNTs and CNFs as compared to CNTs [67] [41].

2.9 Fabrication

2.9.1 Tetrahedral amorphous carbon deposition

Diamond-like carbons are deposited by plasma enhanced chemical vapor deposition (PECVD) or physical vapor deposition (PVD) [57] [70]. The PECVD deposition of DLC requires the use of hydrogen [70]. In this chapter PVD methods for deposition of ta-C are presented in greater detail. For a thorough review on DLC and its deposition the reader is advised to consult reference [57].

The formation of the high sp^3 bonding configuration of ta-C requires high energies of impinging particles forming the film. The growth is assumed to take place through subplantation, instead of condensation as is the case with DLC. [70] Maximum sp^3 fraction can be obtained with ion energies of 100 eV. Below or above this value the sp^3 content starts to fall [57]. The high energies required to deposit non-hydrogenated ta-C films can be achieved with cathodic arc, pulsed arc, laser controlled arc, pulsed laser deposition and mass selected ion beams [70].

In cathodic arc deposition an arc strikes a small, 1–10 µm, spot on the cathode. The large current density causes an explosive emission process, creating both particulates and plasma. [57] The arc can be continuous or pulsed. In pulsed laser deposition the carbon is ablated with short, intense energy pulses from excimer lasers. Pulsed lasers can also cause local overheating resulting in microspalling of the target. As in cathodic arc deposition this causes micron scale macroparticles to be ejected, which cause significant roughening of the deposited film. [57] [70] In cathodic arc deposition the amount of macroparticles can be lowered by filters, in which case the deposition method is called filtered cathodic arc. Generally the filters remove macroparticles by electromagnetically guiding the cathodic arc plasma through a single bend or S-bends. [57] [58]

In situ nitrogen doping can be used to increase the sp^2 fraction of the film. The increase in electrical conductivity is, however, limited. The increased sp^2 clustering also increases the occurrence of pinholes in the film. This limits the usefulness of nitrogen-doped ta-C with films thicknesses below 60–70 nm. [8] [71] Another challenge is the large residual compressive stress, which limits the thickness of the film. The adhesion is commonly

improved by carbide-forming adhesion layers such as Si, Cr, W and Ti. Substrate bias can also be applied to reduce the residual stress of ta-C films. [57]

2.9.2 Synthesis of reduced graphene oxide

Several methods for synthesizing graphene have been reported, including "peeling-off" highly oriented pyrolytic graphite (HOPG), epitaxial growth on Si, chemical vapor deposition (CVD), intercalation of small molecules in a graphite lattice and exfoliation with thermal shock or ultrasonication, and "unzipping" of CNTs. [11] [72] Several extensive reviews on the synthesis methods and the properties of graphene exist, including [73–75], and such a review is therefore not attempted here. Instead focus is given to synthesis by oxidation of graphite, exfoliation, and chemical reduction, as this method will be used to synthesize chemically reduced graphene in this work.

Most methods of synthesis can produce individual graphene sheets with high yield of 90 %. The graphene monolayers do, however, tend to stack and form multi-layered graphene, also known as stacked graphene nanoplatelets (GNPs). It should be noted that the majority of material produced in bulk quantity by the above methods has a multi-layered structure, and should therefore be regarded as GNP. [11] In most cases bulk quantities of graphene oxide is produced by Hummers' and Offerman's method [76], which involves oxidizing graphite powder and subsequent sonication to produce monolayer sheets of graphene oxide (GO). The graphene oxide is then reduced to produce reduced graphene oxide (rGO), increasing the carbon to oxygen atomic ratio C/O ratio and at least partially restoring the aromatic structure. [74]

Several different reducing agents have been used for reduction of GO, including hydrazine [77], hydroquinone [78], sodium borohydride [79], ascorbic acid [80] and many others [81]. In addition thermal treatments have also been applied as efficient low cost reduction method for removal of oxygen containing functionalities [74]. Several groups have also reported electrochemical reduction of GO (ERGO) [82]. Table 2 shows the relative abundance of oxygen containing groups in GO and rGO after different reduction processes.

Table 2. Relative abundance of oxygen containing moieties on graphene produce by different methods.

Material	Reductant/ Reduction method	COOR	C=O	C–O	C–C (defect/sp^3)	C–C (sp^2)	Reference
GO	Modified Hummer's	4.00	15.84	65.98	14.18		[82]
GO	Hummer's	4.46	26.36	25.62	27.49	16.07	[83]
CRGO	Hydrazine vapor	4.00	9.01	19.03	40.01	27.95	[83]
ERGO	CV	3.05	6.75	10.93	18.86		[82]
ERGO	Cathodic reduction	0.48	0.67	3.37	46.62	48.86	[83]

Of the above methods the cathodic reduction seems to give the highest C/O ratio. The chemical reduction of GO with L-ascorbic acid is of interest for in vivo detection of DA, as AA acid is present in concentrations on the order of 0.5 mM in the extracellular fluid in the brain [3]. The chemical reactivity between oxygen containing functionalities present in GO may also provide catalysis for electrochemical oxidation of AA, increasing the selectivity of towards DA. Oxidative treatments of CNTs and CNFs have been shown to catalyze the electrochemical oxidation of AA [14] [68]. The oxygen containing functional groups have also been shown to facilitate the adsorption of DA on the surface of carbon electrodes [29].

3 Experimental

3.1 Synthesis of reduced graphene oxide

GO was prepared from synthetic graphite powder by modified Hummer's method by D.Sc. Vivek Singh. In this process 5 ml concentrated H_2SO_4 was heated to 90 °C in a 300 ml beaker. 1 g $K_2S_2O_8$ and 1 g P_2O_5 was added under stirring. The stirring was continued until all reactants had completely dissolved after which the mixture was cooled to 80 °C. 1 g synthetic graphite powder was added to the prepared H_2SO_4 solution. This mixture was kept at 80 °C for 4.5 hours. Subsequently the mixture was diluted with 200 ml of deionized (DI) water and left overnight. The mixture was then filtered and washed to remove all traces of acid after which the solid was transferred to a Petri dish and allowed to dry in air overnight. For the oxidation, 46 ml H_2SO_4 was placed into a round bottom flask and cooled down to 0 °C by means of an ice bath. The pretreated graphite was then added to the acid and stirred. 6 g $KMnO_4$ was added slowly and allowed to dissolve under stirring. The temperature was closely monitored so as not to allow the temperature of the mixture to rise above 5 °C. This mixture was then allowed to react at 35 °C for 2 hours before addition of DI water (92 ml). The mixture was diluted with 280 ml DI water under continuous stirring during 2 hours.

After the dilution, 5 ml of 30% H_2O_2 was added to the mixture resulting in a brilliant yellow color along with gas formation. The mixture was allowed to settle for at least a day after which the clear supernatant was decanted. The remaining mixture was centrifuged and washed with 10% HCl solution followed by DI water to remove the acid and the product was dried at room temperature. Finally, the graphite oxide was dispersed into water by ultrasonication to get GO suspension.

The reduction of the GO was carried out with ammonia. 1 ml of liquor ammonia solution (HN_4OH) was added to 10 ml of GO solution and stirred for 10 min. The rGO was then collected by filtration and washed multiple times with DI water. Finally the rGO was dispersed in DI water to achieve a final concentration of 10 mg ml^{-1}.

3.2 Electrode fabrication

The electrodes were fabricated on highly conductive (0.001–0.002 Ω cm) p-type (100) silicon. Prior to deposition the Si wafers were RCA cleaned and ultrasonicated in highly pure acetone. A 20 nm Ti intermediate layer was deposited by direct current magnetron sputtering (DC-MS) on all electrodes. The subsequent ta-C top layer with thicknesses of 2, 3, 4, 7, 14, and 30 nm was deposited by filtered cathodic vacuum arc (FCVA). Table 3 shows the used deposition parameters for both Ti interlayer and ta-C deposition.

Table 3. Deposition parameters of Ti intermediate layers and ta-C top layers.

Material	Deposition method	Pressure (Torr)	Power/ Arc voltage	Distance from target/cathode
Ti	DC-MS	$1 \cdot 10^{-3}$	100 W	22 cm
ta-C	FCVA	$1 \cdot 10^{-6}$	400 V	22 cm

Both DC-MS and FCVA systems were installed in a 125 l cylindrical stainless steel vacuum chamber. The chamber was equipped with a dry scroll vacuum pump (Edwards XDS10) and a Cryo-Torr (Helix Technology Corporation) cryo pump, and it was pumped down to a vacuum of $1 \cdot 10^{-6}$ Torr prior to all depositions. A high vacuum throttle was used to achieve the low vacuum needed for DC-MS. The system was equipped by two MS systems with a 2 inch Ti and 4 inch Al targets (Kurt J. Lesker Company), and a DC generator (DCO2 BP). The targets were pre-cleaned by sputtering for 120 sec with a discharge power of 200 W prior to deposition. Shutters were used for MS deposition time control.

The FCVA system was equipped with two 99.997 % graphite rods (Goodfellow) with a diameter of 6.35 mm. The graphite cathodes were mounted in a cylindrical anode and a 60° bent magnetic filter was used to reduce macroparticle contamination. A 2.6 mF capacitor bank was charged to 400 V. The arc current pulses were triggered with 1 Hz frequency, and had an amplitude of 0.7 kA and a pulse width of 0.6 ms. The pressure in the chamber during deposition was below $1.3 \cdot 10^{-4}$ Pa.

The deposition rates of both DC-MS and FCVA were obtained by depositing a calibration series of metals and ta-C, respectively. The film thicknesses were measured with a Dektak XT profilometer, and subsequently thickness calibrations curves for deposition time and number of pulses for DC-MS and FCVA, respectively, were made.

The backside of the fabricated samples was subsequently contacted to a copper plate. The copper plate and sample were covered with teflon tape, with a pre-made hole with a 6 mm diameter. The tape covered the sample and copper plate in such a way that the electrolyte could reach contact only with the 6 mm diameter hole.

Some of the obtained Ti/ta-C bilayer electrodes with 7 nm ta-C top layer were modified with reduced graphene oxide (rGO). The modification was carried out by drop casting. 40 µl of rGO water solution (10 mg/ml) was pipetted onto the exposed area of a premade Ti/ta-C bilayer electrode. The rGO solution was subsequently dried in a vacuum oven at 50 °C for 10 min. Electrodes modified by 1, 3 and 5 drops of rGO solution were prepared. The electrodes modified by 3 and 5 drops of rGO solution were made by repeating the pipetting and drying steps 3 or 5 times. Some rGO modified electrode were subsequently treated with 10 M nitric acid, by submerging the electrode in the acid for 5 min.

4.3 Characterization

The bonding configuration of the ta-C and rGO was characterized by means of visible Raman spectroscopy (WITec alpha 300 spectrometer). All carbon films give Raman spectra with a G peak centered around 1560 cm^{-1} and a D peak around 1360 cm^{-1}. Both these peaks are caused by the sp^2 fraction, because the excitation resonates with π states. The G peak is due to bond stretching of the pairs of sp^2 atoms in rings and chains, while the D band is due to breathing modes of sp^2 atoms in rings. [84] Nevertheless the I(D)/I(G) ratio correlates with sp^3/sp^2 ratio, band gap value, and film density [84] [61]. In the case of rGO the I(D)/I(G) ratio is a measure of reduction of rGO, as the intensity of the G band is known to be that of the D band for GO, while the opposite is true for rGO. [77] The Raman spectra were acquired with a laser wave length of 532 nm and spectrum wave number of 450 to 3900 cm^{-1}. The used exposure time and number of accumulation was 0.5 s and 10 s, respectively.

The rGO electrodes were also subjected to scanning electron microscopy (SEM) and Fourier transform infrared spectroscopy (FT-IR) analysis. For FT-IR analysis separate GO and rGO samples were prepared on undoped (100) silicon. The transmission FT-IR spectra were obtained with a Nicolet Manga-IR 750 spectrometer. Both untreated and nitric acid treated rGO samples were analyzed.

4.4 Cyclic voltammetry

The electrochemical properties of the fabricated electrodes were measured with cyclic voltammetry. A Gamry Reference 600 Potentiostat/Galvanostat/ZRA and a three-electrode configuration were used. The reference electrode was Ag/AgCl skinny reference electrode (Sarissa Biomedical ltd., Coventry, UK) and the counter electrode was glassy carbon. From here on any reported potential is always relative to the Ag/AgCl reference electrode, unless stated otherwise. Water windows were measured both in 0.15 M sulfuric acid and phosphate buffered saline (PBS) solution at a sweep rate of 400 mV/s. The pH values of the PBS solution and sulfuric acid was 7.4 and 0.90, respectively. In addition the capacitive currents were measured in 0.15 M sulfuric acid. Based on the measured currents the apparent double layer capacitance was calculated.

The outer-sphere redox system ferrocenemethanol (FcMeOH) was used to define the electron transfer rate of the electrodes. The ferrocene redox couple is known to be an outer sphere redox system, which is insensitive to electrocatalytic or adsorption steps [48]. The 1 mM FcMeOH solution was prepared by dissolving 0.0223 g of 97 % ferrocenemethanol (Sigma-Aldrich, St. Louis, USA) in 100 mL 0.15 M sulfuric acid (Merck kGaA, Darmstadt, Germany). FcMeOH measurements were carried out at sweep rates of 50 and 400 mV/s for each ta-C and rGO modified electrode.

The detection limits and kinetics of DA at the electrodes were determined at different DA concentrations. A 10 mM dopamine solution was prepared, by dissolving dopamine hydrochloride (Sigma-Aldrich, St. Louis, USA) in 100 mL. The obtained DA solution was then diluted to concentrations ranging from 1 mM to 100 nM. In addition the selectivity was studied by preparing solutions with 1 mM ascorbic acid and varying concentrations of DA. 0.1778 g 99 % L-ascorbic acid (Sigma-Aldrich, St. Louis, USA) was dissolved in 100 mL PBS solution to obtain a 10 mM stock solution. DA solutions with 10 mM, 100 µM,

and 10 μM concentrations were prepared as above. 5 mL of both AA and DA solutions were then diluted in 40 mL PBS solution to achieve solutions with 1 mM AA and DA concentrations from 1 μM to 1 mM.

Prior to all measurements the solutions were saturated with N_2 for 5 min and during measurement the cell was kept at N_2 atmosphere. In addition the DA and AA was dissolved and diluted in N_2 saturated PBS solutions. All measurements were carried out at room temperature and the FcMeOH as well as the DA solutions were prepared on the day of the measurement to prevent oxidation from occurring.

4 Results and discussion

4.1 Optimization of ta-C thickness

4.1.1 Raman spectroscopy

The bonding configuration of ta-C was studied with Raman spectroscopy. The samples with 2 and 3 nm ta-C thickness were too thin and did not produce a reasonable signal for analysis. The low signal intensity and low signal to noise ratio cause the individual contributions of the D and G bands for ultrathin 1–10 nm to become obscure. The Raman spectra of the 4, 7, 14, and 30 nm ta-C are shown in Figure 7 a) and the I(D)/I(G) ratio as well as the G peak position a function of ta-C thickness in Figure 7 b).

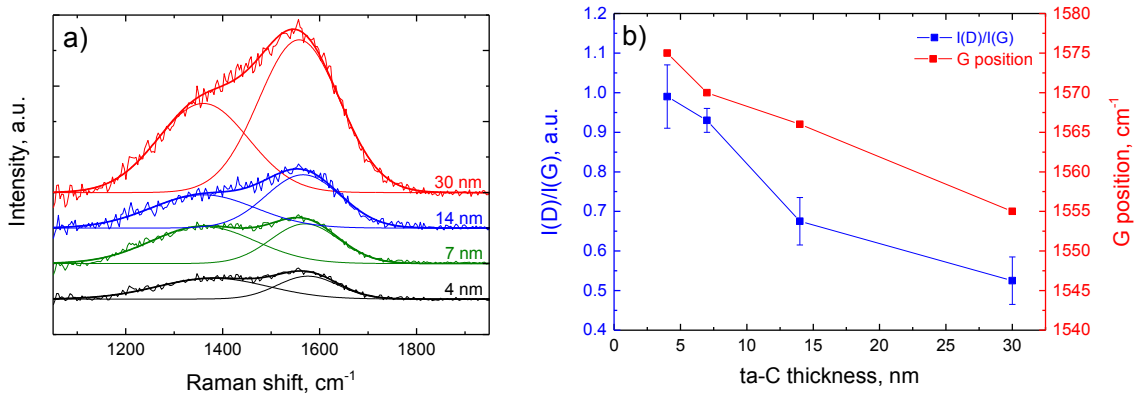

Figure 7. a) Raman spectrum of different ta-C thicknesses and b) I(D)/I(G) and G band position dependence on ta-C thickness.

Figures 7 a) and b) show that the I(D)/I(G) ratio decreases with increasing ta-C thickness. A shift in the G peak position towards lower wave number with increasing thickness was also observed. These findings indicate that the sp^2 fraction decreases with increasing film thickness. These results are in good agreement with what has been previously reported for ultrathin ta-C films. [61] [62] To achieve an I(D)/I(G) ratio of around 0.25, associated with high sp^3 content ta-C, a film thickness of approximately 50 nm is required [61].

4.1.2 Cyclic voltammetry

4.1.2.1 Water window and double layer capacitance measurements

The electrochemical properties of the ta-C top layer were studied with cyclic voltammetry. Here the effect of ta-C top layer thickness on the electrochemical properties of the electrode is studied. First cyclic voltammetry with cycling speed 400 mV/s was carried out in both mild H_2SO_4 and PBS to determine the water windows. A current threshold of 200 µA was used. The apparent double layer capacitance was also determined in H_2SO_4. Figure 8 shows the cyclic voltammograms for the bare Ti as well as for the electrodes with varying ta-C thickness in mild H_2SO_4 and PBS with a cycling speed of 400 mV/s.

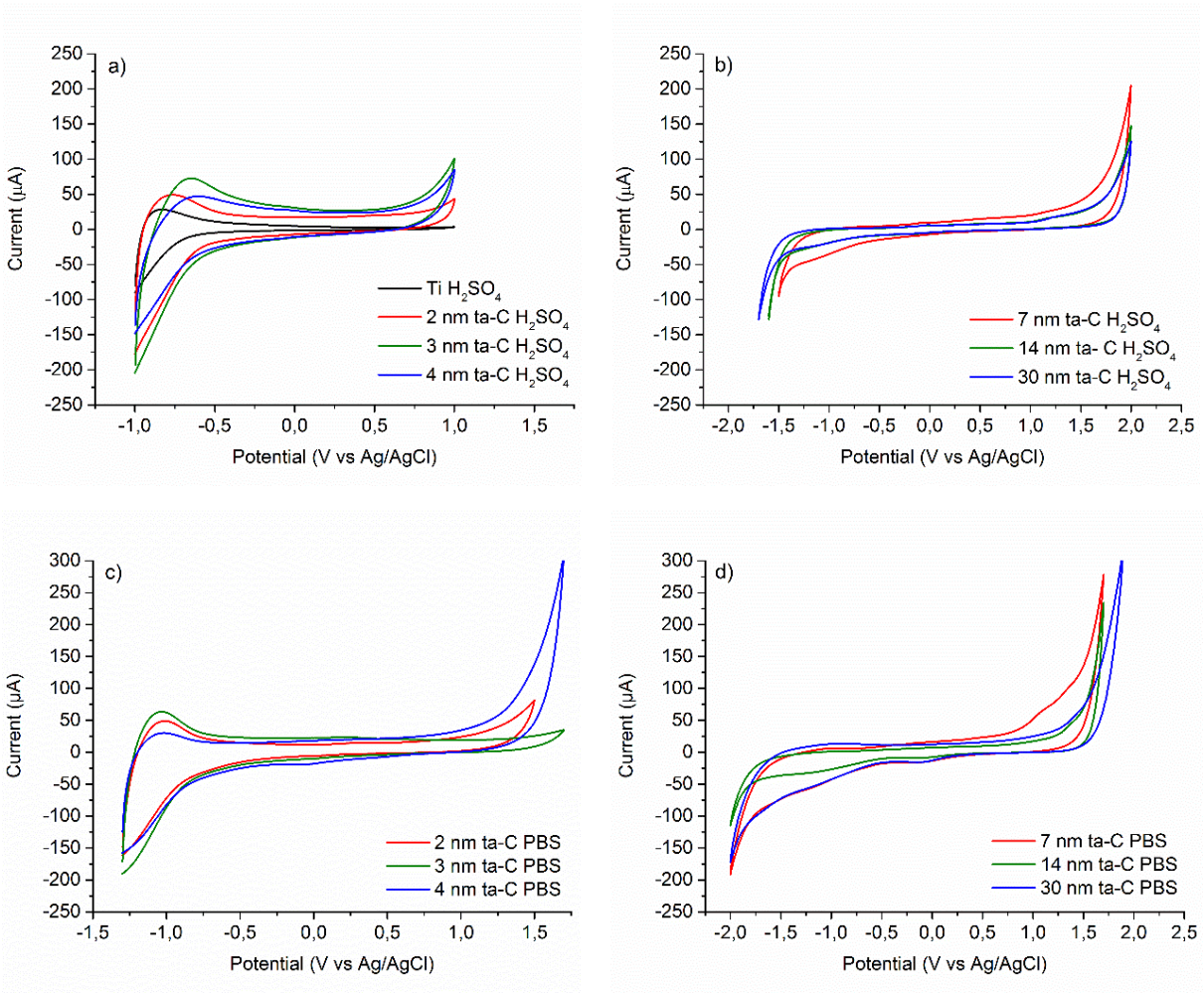

Figure 8. Potential windows in H_2SO_4 of a) 2 ,3 and 4 nm ta-C electrodes and b) 7, 14 and 30 nm ta-C electrodes, and in PBS of c) 2,3 and 4 nm ta-C electrodes and d) 7, 14 and 30 nm ta-C.

It is evident that for the three thinnest ta-C top layer electrodes passivation of Ti can be observed. As seen from Figure 8 a) and c) this is the case in both mild H_2SO_4 and PBS solution, respectively. The width of the water windows in both mild sulfuric acid and PBS solution was observed to grow as the ta-C thickness increased. The reduction of Ti can be seen to occur at more negative potentials in the PBS solution, where onset of reduction occurs at around –1 V as compared to approximately –0.7 V in the sulfuric acid. The anodic current likely indicates passivation of the Ti on the forward scan. In any case the 2, 3 and 4 nm thick ta-C films provide poor corrosion protection for the underlying Ti both at physiological and acidic pH of 7.4 and 0.9, respectively. The observed electroactivity of Ti and hence the absence of a flat double layer region as well as poor stability for the electrodes with ta-C thickness below 7 nm makes them poorly suitable for electrochemical detection of DA. As high stability and facile heterogeneous electron transfer rates are required of mediating layers, these electrodes are not ideal for modification with rGO.

For the 7, 14 and 30 nm ta-C electrodes redox activity of Ti was not observed in mild H_2SO_4 (Figure 8 b) or PBS (Figure 8 d). For the more stable electrodes with ta-C top layer of 7 nm and above the apparent double layer capacitance was determined at -1, 0, and +1 V, with cycling speeds of 50 and 400 mV/s. The measurements were carried out in 0.15 M sulfuric acid. Geometric area of the electrodes and the difference between the anodic and cathodic current densities was used to calculate the capacitances with equation 2. The determined potential windows and capacitance values are presented in Table 3.

Table 3. Potential window ΔE sweep and calculated double layer capacitance values for electrodes T360, T720 and T1680.

ta-C thickness [nm]	Potential window, ΔE_{sweep} [V]	Capacitance, [µF/cm^2]
7	3.5	145±39
14	3.6	94±37
30	3.7	78±20

All the thicker ta-C films were found to be stable and have relatively wide water windows. The absence of a real flat double layer region in the measured voltammograms indicates with high probability the presence of faradic reactions, in addition to pure charging current. This is especially the case with the 7 nm ta-C electrode, for which the capacitance can be seen to be larger than for the other two. IR drop may also contribute to the high measured double layer capacitance values. Therefore, the double layer capacitances are referred to as pseudocapacitances. The capacitance can be seen to decrease with increasing ta-C thickness. This is likely due to the increasing sp^2 nature of the films with decreasing thickness, as was shown by the Raman spectroscopy measurements. The measured double layer pseudocapacitances are reasonably small for all electrodes. Significantly smaller capacitances have, however, been reported for ta-C electrodes. Liu and coworkers [85] reported a capacitance of only 1.02 $\mu F/cm^2$ for a ta-C film deposited by FCVA. The ta-C thickness was, however, 100 nm and the capacitance was measured by means of EIS. More accurate characterization of the Ti/ta-C bilayer electrode and the effect of ta-C thickness on the apparent double layer capacitance still needs to be carried out.

4.1.2.2 Ferrocenemethanol

The ferrocene redox couple was used to determine the electron transfer properties of the electrodes as function of ta-C film thickness. In a system with reversible electron transfer the peak separation is 59 mV regardless of the applied cycling rate. In addition anodic and cathodic peak current ratio Ip_a/Ip_c should not deviate from unity. The uncompensated resistance of the electrodes causes the peaks to shift and the ΔE_p to grow. For this reason IR compensation with 80 % of the uncompensated resistance, R_u was applied. All electrodes were measured three times with both cycling speeds of 50 and 400 mV/s. The voltammograms and the average results of these measurements are shown in Figure 9 and Table 4.

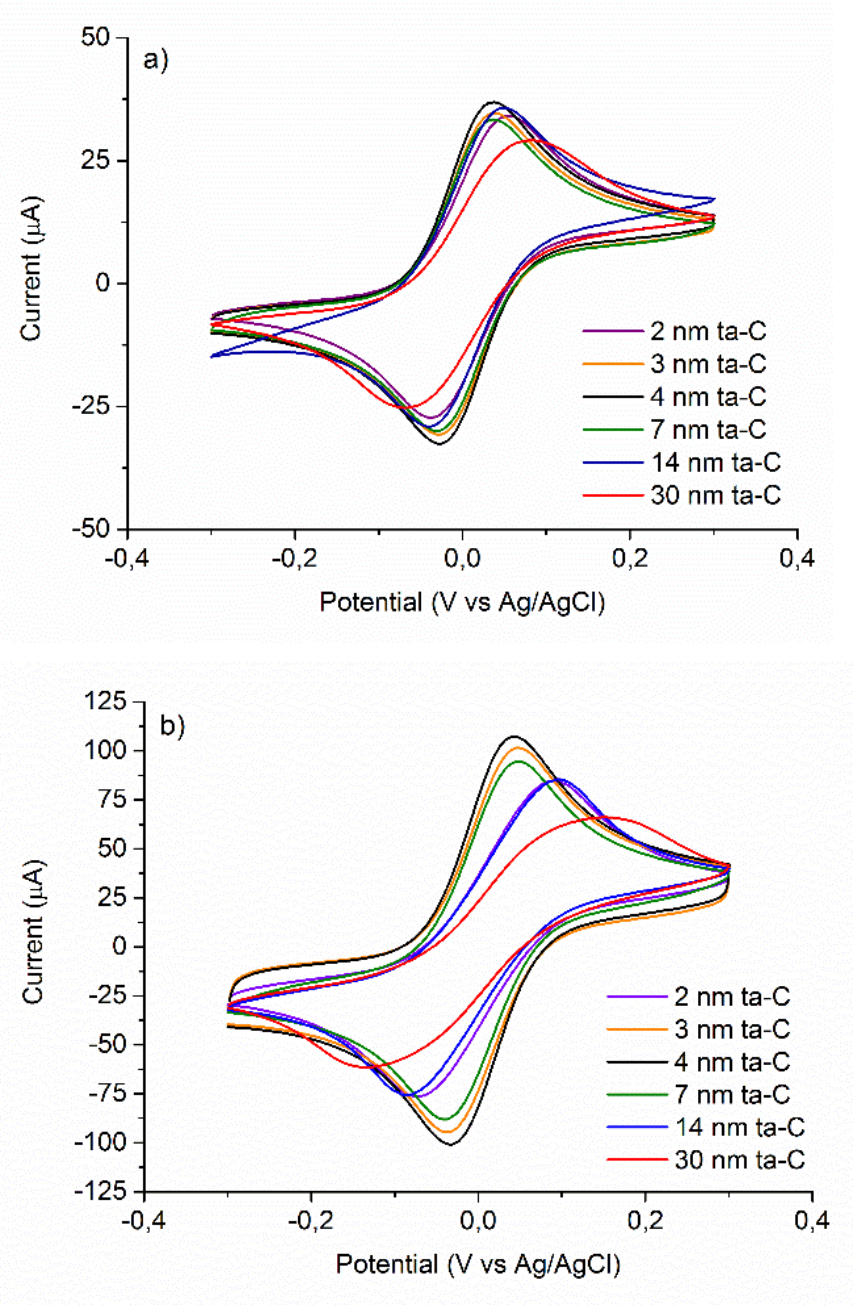

Figure 9. Cyclic voltammograms of different ta-C top layer thicknesses at cycling speed of a) 50 mV/s, and b) 400 mV/S.

Table 4. Separation of FcMeOH oxidation and reduction peak potential, oxidation and reduction peak current ratio at cycling speeds of 50 mV/s and 400 mV/s for with different ta-C top layer thickness.

ta-C thickness [nm]	ΔE_p FcMeOH [mV] (50 mV/s)	Peak current ratio i_{pa}/i_{pc} (50 mV/s)	ΔE_p FcMeOH [mV] (400 mV/s)	Peak current ratio i_{pa}/i_{pc} (400 mV/s)
2	92 ± 27	1.01 ± 0.01	128 ± 19	1.02 ± 0.01
3	62 ± 2	1.03 ± 0.003	71 ± 3	1.04 ± 0.004
4	62 ± 1	1.02 ± 0.01	70 ± 2	1.03 ± 0.001
7	61 ± 1	1.01 ± 0.01	70 ± 7	1.03 ± 0.003
14	76 ± 4	0.94 ± 0.01	124 ± 30	1.02 ± 0.005
30	148 ± 1	1.01 ± 0.001	283 ± 3	1.06 ± 0.04

From Figure 9 it can be seen that the lowest ΔE_p values were obtained with the 4 and 7 nm electrodes and therefore show the fastest rate of hetero electron transfer. The same values are, however, not obtained with the sweep rates of 50 and 400 mV/s. The peak current ratio is very close to unity for all electrodes at both cycling speeds. The observed behavior of all the electrodes is quasireversible and the electron transfer rate is not fast enough to achieve a completely Nernstian system. It should, however, be noted that for the 4 and 7 nm electrodes the IR compensated ΔE_p values only increase from 62 mV and 61 mV to 70 mV for both electrodes when cycling speed was increased from 50 to 400 mV/s. For the other electrodes the change is much clearer and electron transfer was significantly slower at cycling rates of 400 mV/s, as compared to 50 mV/s.

These results are in agreement with the conductive AFM results and band gap measurements previously reported by Protopopova et al. [63], where conductivity was found to increase and band gap to decrease with decreasing ta-C thickness. As with the results presented here this trend continued down to 7 nm ta-C thickness. In chapter 4.2.2.1 evidence for electroactivity of Ti for the 2, 3 and 4 nm ta-C electrodes was presented. The observed increase in band gap value and reduced conductivity reported earlier together with deterioration of heterogeneous electron transfer especially at thicknesses below 4 nm is proposed to be caused by a formation of titanium dioxide layer at the Ti/ta-C interface.

4.1.2.3 Sensitivity towards dopamine

To find out if the determined electron transfer rates correlate with DA biosensor performance, the sensitivity of the electrodes towards dopamine was determined. Figure 10 shows the results for each ta-C electrode with DA concentrations of 0.1 to 100 µM.

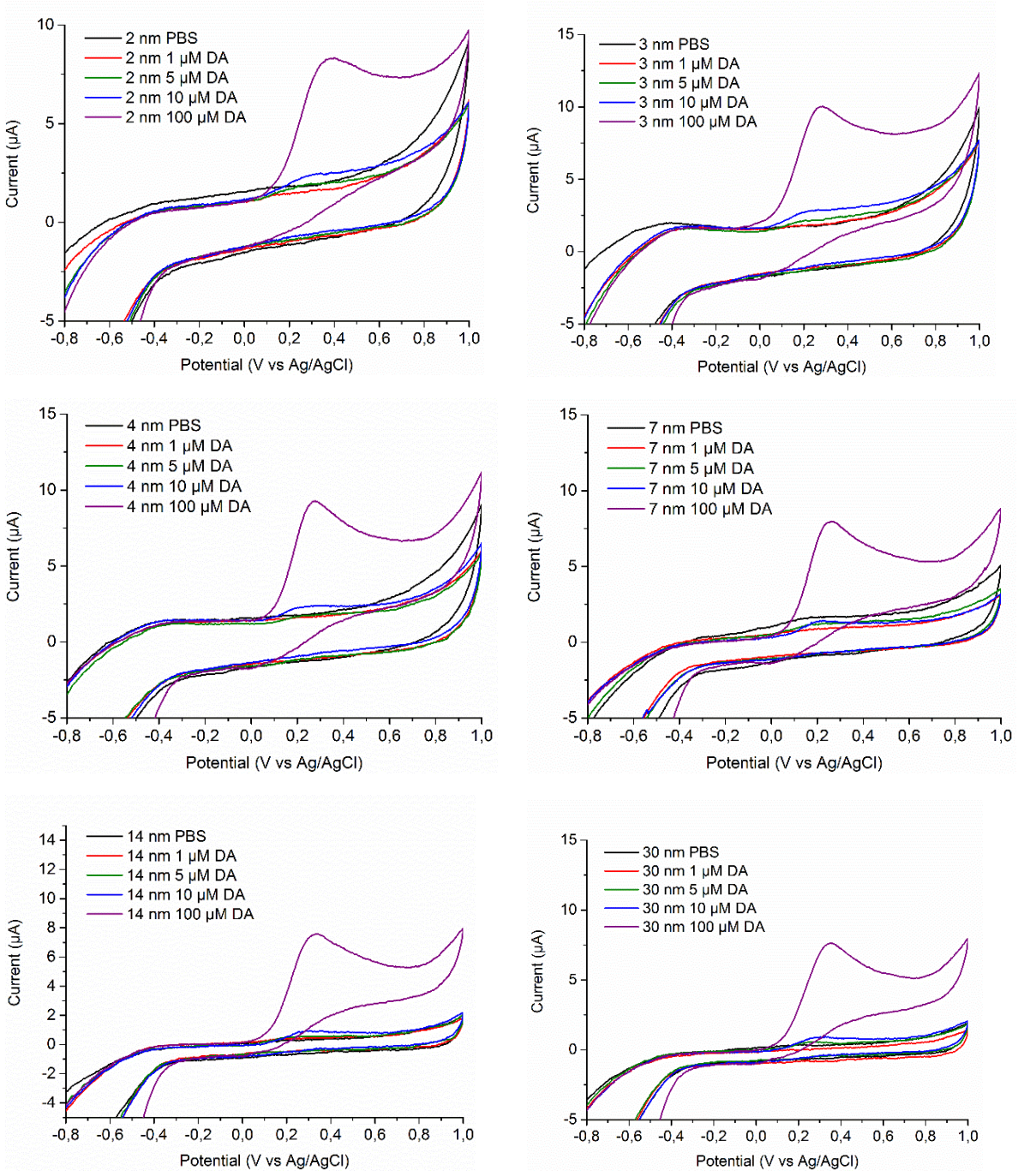

Figure 10. Cyclic voltammograms of different thickness ta-C electrodes in DA solutions with concentrations from 1 to 100 µM.

As can be seen in Figure 10 all electrodes give close to similar response to DA. In the region before the onset of DA oxidation a clear decrease in capacitive current can be observed for the thicker 7, 14 and 30 nm electrodes as compared to the 2, 3 and 4 nm electrodes. The sensitivity towards DA is relatively unaffected by the ta-C thickness. There seems to be no clear correlation between detection limit and rates of heterogeneous electron transfer determined above, as all the electrodes are able to detect 5 μM DA concentration.

The bilayer electrode with 7 nm ta-C top layer has earlier been reported to have a detection limit of 1 μM [10]. This work was, however, unable to repeat these results. In addition the 30 nm ta-C electrode was able to detect 5 μM, and showed the same detection limit as the 7 nm ta-C electrode. Laurila et al. [10] concluded that the difference in performance was at least partially due to different Ti underlayer deposition method. The results presented here support this conclusion as the performance of the 30 nm ta-C top layer electrode is improved when the Ti under layer is deposited by means of DC-MS as opposed to by means of FCVA. It should be noted, however, that the current response shows slight deterioration at thicknesses above 7 nm.

Interestingly the thickness was also found to have an effect on the kinetics and the reversibility of the DA/DAQ redox couple. Figure 11 shows the voltammograms of the ta-C electrodes in 1 mM DA solutions. The determined peak potential separation, ΔE_p and oxidation peak current, Ip_a values are shown in Table 5.

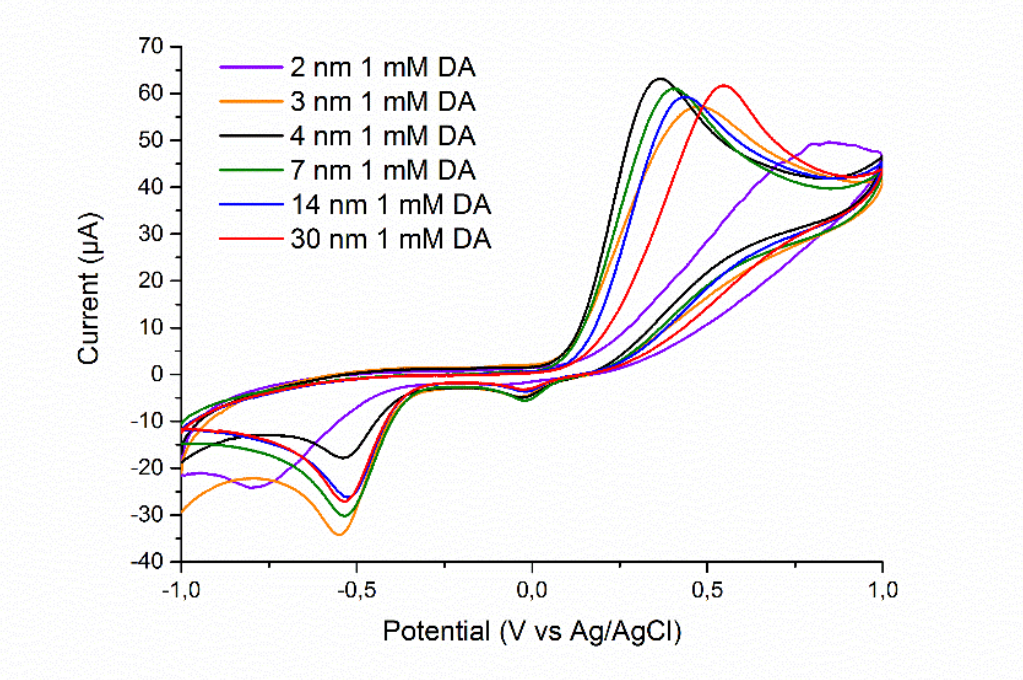

Figure 11. Cyclic voltammogram of different thickness ta-C electrodes in 1 mM DA solution.

Table 5. Peak potential separation ΔE_p and oxidation peak potential Ip_a of different thickness ta-C electrodes in 1 mM DA solution

ta-C thickness (nm)	ΔE_p DA (mV)	I_{pa} (µA)
2	960	46.11
3	503	54.82
4	377	60.51
7	422	60.08
14	448	57.92
30	562	60.46

Two reduction peaks can be observed on the backward scan for all electrodes, except for the 2 nm electrode, which shows no clear peak for reduction of DAQ. Oxidation peak currents were close to identical for the 4 to 7 nm electrodes. The 2 and 3 nm electrodes showed lower peak current values, indicating lower active surface area. The ΔE_p were observed to decrease with decreasing ta-C thickness down to 4 nm, after which the peak potential separation increased again for the 2 and 3 nm electrodes. The 4 and 7 nm electrodes can be seen to have the smallest ΔE_p values of 377 and 422 mV, respectively.

The kinetics of the DA/DAQ redox couple correlate well with heterogeneous electron transfer.

The kinetics of these ta-C electrodes with DA is still relatively sluggish compared to what has been reported for more electroactive carbon materials. The detection limit is also not sufficiently low to be able to detect DA basal levels or transients. The relatively facile heterogeneous electron transfer and chemical stability combined with reasonably low capacitive currents makes this bilayer electrode an excellent mediating layer for modification with rGO. Even though the 4 nm electrode showed most facile kinetics of the DA/DAQ redox couple the issue of Ti electroactivity and long term stability makes the 7 nm ta-C electrode more fitting for rGO modification.

4.2 The optimized structure (Ti/7nm ta-C)

4.2.1 The effect of scan rate

In light of the above findings, the 7 nm ta-C top layer electrodes were employed to determine the reaction mechanism of DA in CV experiments. In addition the effect the scan rate on both DA and AA systems were evaluated.

In Figure 12 and 13 the first and second cycle, respectively, of CV measurements with varying scan rates with 1 mM DA in PBS solutions are presented. Here the primary interest was determining the effect of scan rate on the primary DA/DAQ redox couple. The voltammograms, however, also give information about the reaction mechanism of DA on the applied electrode. To achieve more clear effect on the oxidation of LDAC to DAC a larger measurement window could have been used.

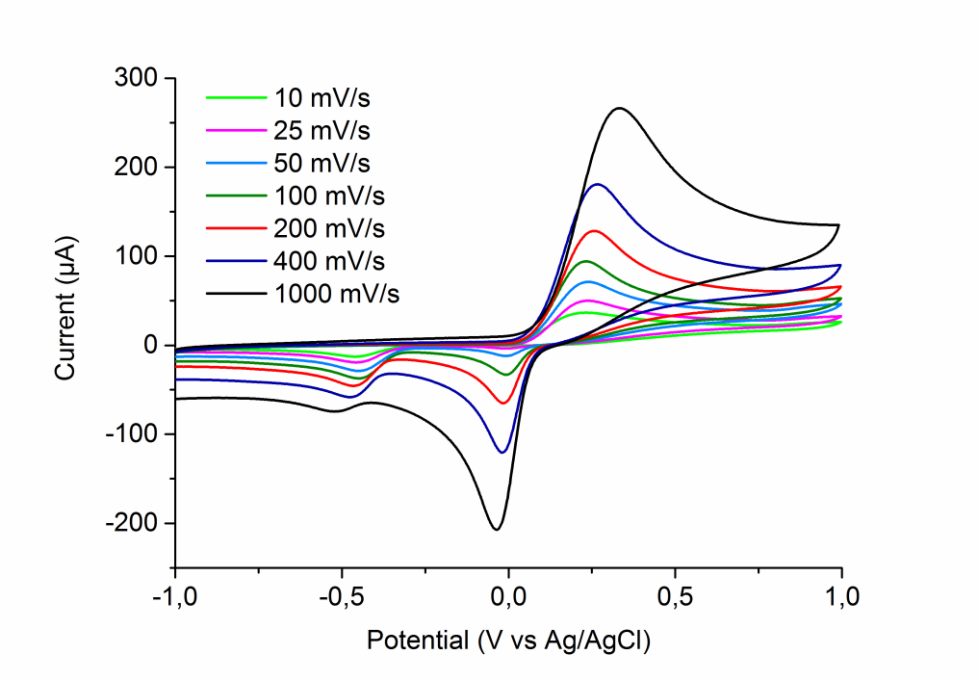

Figure 12. Cyclic voltammogram of first cycles of 7 nm ta-C electrode with different scan rates ranging from 10 to 1000 mV/s.

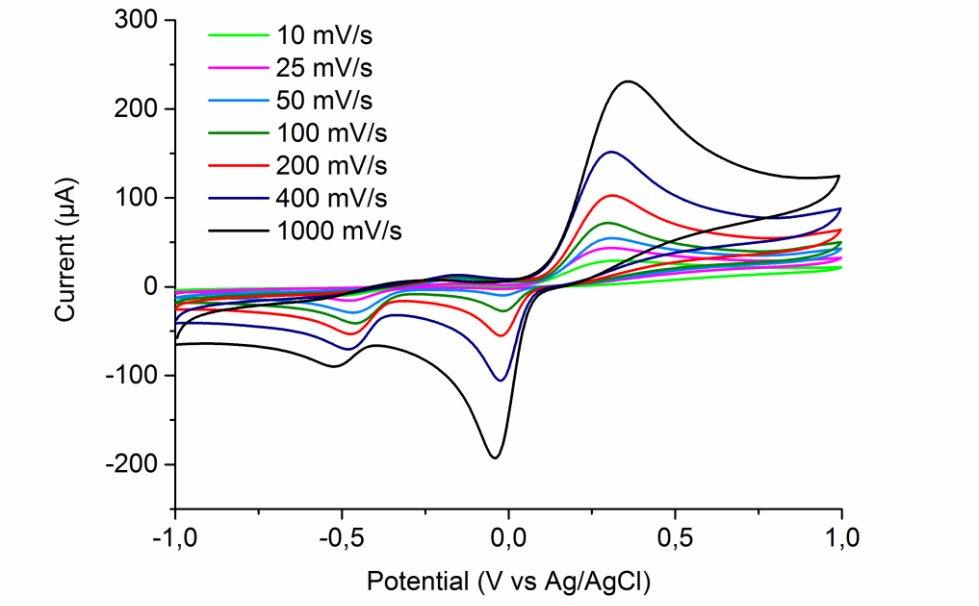

Figure 13. Cyclic voltammogram of second cycles of 7 nm ta-C electrode with different scan rates ranging from 10 to 1000 mV/s.

During the first cycle the oxidation of DA to DAQ can be observed. DAQ subsequently reacts chemically to form leucodopaminechrome (LDAC) [27]. After electrochemical

oxidation the continued potential sweeping leads to an overpotential, which causes immediate electrochemical oxidation of LDAC to DAC. A peak like feature can be observed for this reaction at a potential around 1.2 V [9]. Owning to the DAQ and DAC present on the electrode surface, two reduction peaks were observed on the reverse scan. The first peak is related to the reduction of DAQ to DA, and the latter to reduction of DAC to LDAC. The increase in scan rate clearly shows an increase in the peak current of the reduction peak corresponding to reduction of DAQ, whereas only minor increase in the DAC reduction peak was observed. This is attributed to the faster scan rate, leading to less time passing before the reduction potential of DAQ is reached, and allows for less time for the chemical reaction of DAQ to LDAQ. The kinetics of this reaction can, however, not be totally outrun even with the scan rate of 1 V/s, in the applied measurement window of -1 V to +1 V.

Figure 14 presents the peak current ratio, Ip_a/Ip_c as function of the scan rate. The Ip_a/Ip_c ratio can be seen to decrease with increasing scan rate, indicating a more reversible reaction at faster scan rates. As can be seen in Figure 13 there is a clear decrease in the peak current ratio with increasing in scan rate. At slow scan rates the reaction is almost totally irreversible. As the scan rate increases the Ip_a/Ip_c ratio approaches unity and the reaction becomes more reversible.

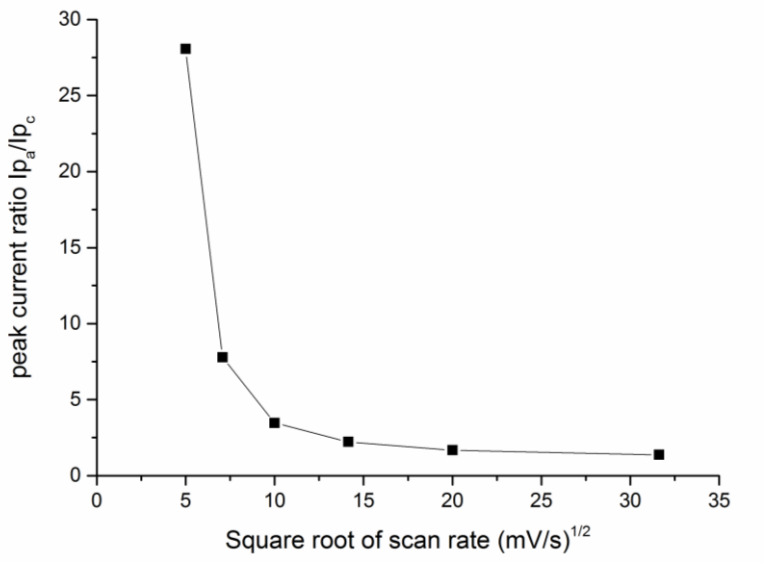

Figure 14. Peak current ratio as function of the square root of scan rate.

This result is expected, as the chemical reaction of DAQ to LDAC has slow kinetics and does not have time to occur when fast scan rates are applied. Therefore as scan rate increases the peak current ratio approaches unity. With the reasonably fast scan rate of 1000 mV/s an Ip_a/Ip_c value of 1.37 was obtained. The deviation from unity is due to the formation of LDAC, as a second reduction peak may still be observed with this scan rate, as can be seen in Figure 12. A further increase in scan rate should be to able further inhibit formation of LDAC.

On the second anodic scan (shown in Figure 12) another oxidation peak related to the oxidation of LDAC to DAC appears. The peak current of the DA oxidation peak is reduced on the second cycle, owing to reduced DA concentration on the electrode surface. Laurila et al. [10] observed a formation of a passivating surface film when cycling speed of 50 mV/s was used with a ta-C electrode. No passivation was observed at a cycling speed of 400 mV/s. It was concluded that the polymerization reaction is not fast enough to occur at this cycling rate. Li et al. [27] observed the same effect when using Au electrodes.

The DA concentration of 1 mM, is orders of magnitude larger than endogenous DA concentrations. Li et al. found that reducing the DA concentration to 100 μM severely inhibited the chemical reaction of DAQ to LDAC. At a DA concentration of 10 μM, only one peak, corresponding to oxidation of DA may be observed. It should also be noted here that the endogenous conditions differ markedly from the single analyte DA system applied here, including the effects of relatively high concentrations of interferents, such as AA and UA.

The effect of the scan rate on the peak current and peak current ratio was also studied. Figure 15 shows the peak currents of both the oxidation and reduction current as function of applied scan rate.

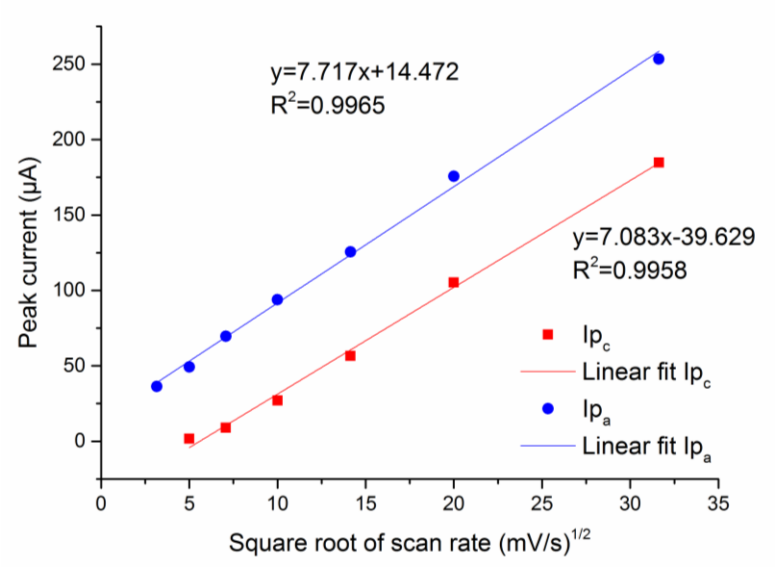

Figure 15. Oxidation and reduction peak currents as function of square root of the scan rate in 1 mM DA solution

The data fits well to a linear model as a function of the square root of the scan rate, indicating that the reaction is under diffusion control [20]. DA is, however, known to require specific adsorption for electrochemical oxidation to occur [29] [30]. As pointed out above the 1 mM DA concentration is several orders of magnitude larger than in vivo concentrations and may provide little information about systems with significantly lower DA concentrations. This concentration is, however, commonly used to study the reaction scheme and kinetics of DA redox reactions. The above findings imply that further studies should be carried out at lower conditions with this electrode.

The effect of the applied scan rate with the ta-C electrode was also studied for AA. Figure 16 a) shows the voltammograms for the CV measurements with 1 mM L-ascrobic acid solution, and b) the peak current as function of the square root of the scan rate.

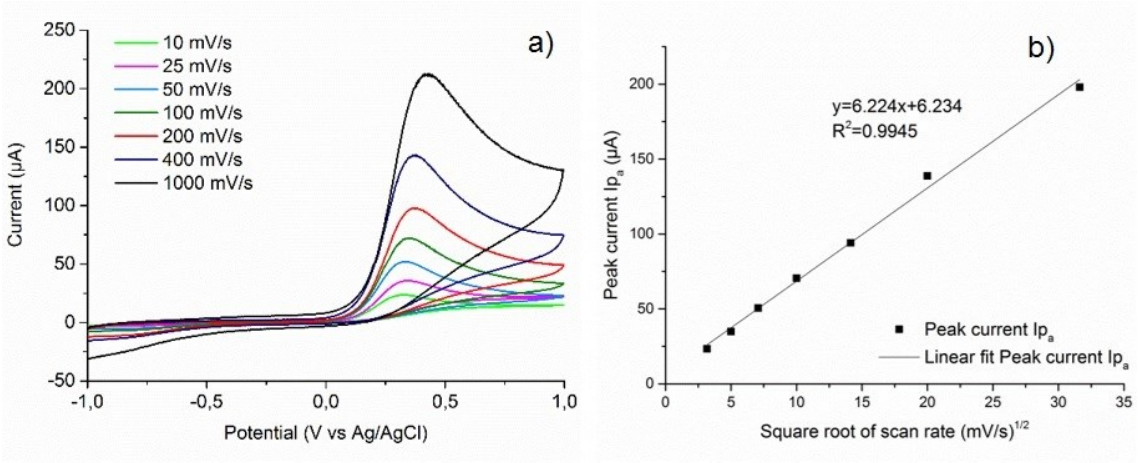

Figure 16. a) Cyclic voltammogram of 7 nm ta-C electrode with different scan rates in 1 mM L-ascorbic acid and b) peak currents as function of scan rate.

The oxidation of AA can be seen to be totally irreversible, as no reduction peak for AA was observed in the experiments, whereas DA can be electrochemically reduced after electrochemical oxidation. The irreversibility of the reaction is caused by a rapid chemical reaction with water as was shown by Ruiz et al. [42]. The peak current was found to be proportional to the square root of the scan rate, indicating that the reaction is under diffusion control [20].

4.2.2 Selectivity towards DA in DA + AA system

The selectivity towards DA was evaluated in the presence of 1 mM L-ascorbic acid. Figure 17 shows the simultaneous CV measurement of the heterogeneous system of AA and DA, as well as the single analyte voltammograms for AA and DA solutions.

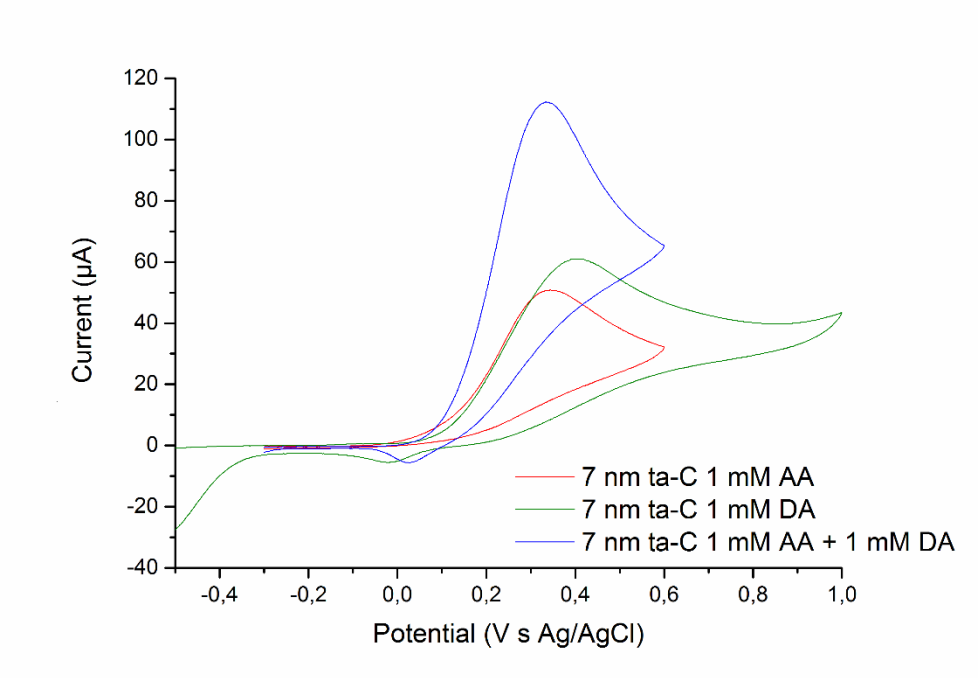

Figure 17. Cyclic voltammogram of 7 nm ta-C electrode in 1 mM AA, 1 mM DA and 1 mM AA + 1 mM DA solution with scan rate of 50 mV/s.

The selectivity of the ta-C electrode towards DA can be seen to be poor in this system, and oxidation peaks of the analytes cannot be distinguished. In the voltammogram of the solutions containing equimolar concentrations of 1 mM DA and AA, a small reduction peak of can be seen. Previous measurements showed that AA does not reduce on the backward scan at the applied scan rate of 50 mV/s. The observed reduction peak is due to reduction of DA on the backward scan. With electrodes, such as the Ti/ta-C bilayer electrode that cannot distinguish between DA and AA the reduction peak of DA may be useful as it could be used to detect DA.

4.3 Reduced graphene oxide modified electrodes

4.3.1 SEM Characterization

Scanning electron microscopy images of the rGO modified electrodes were taken to study the coverage of the ta-C. SEM images for the rGO modified electrodes are presented in Figure 18.

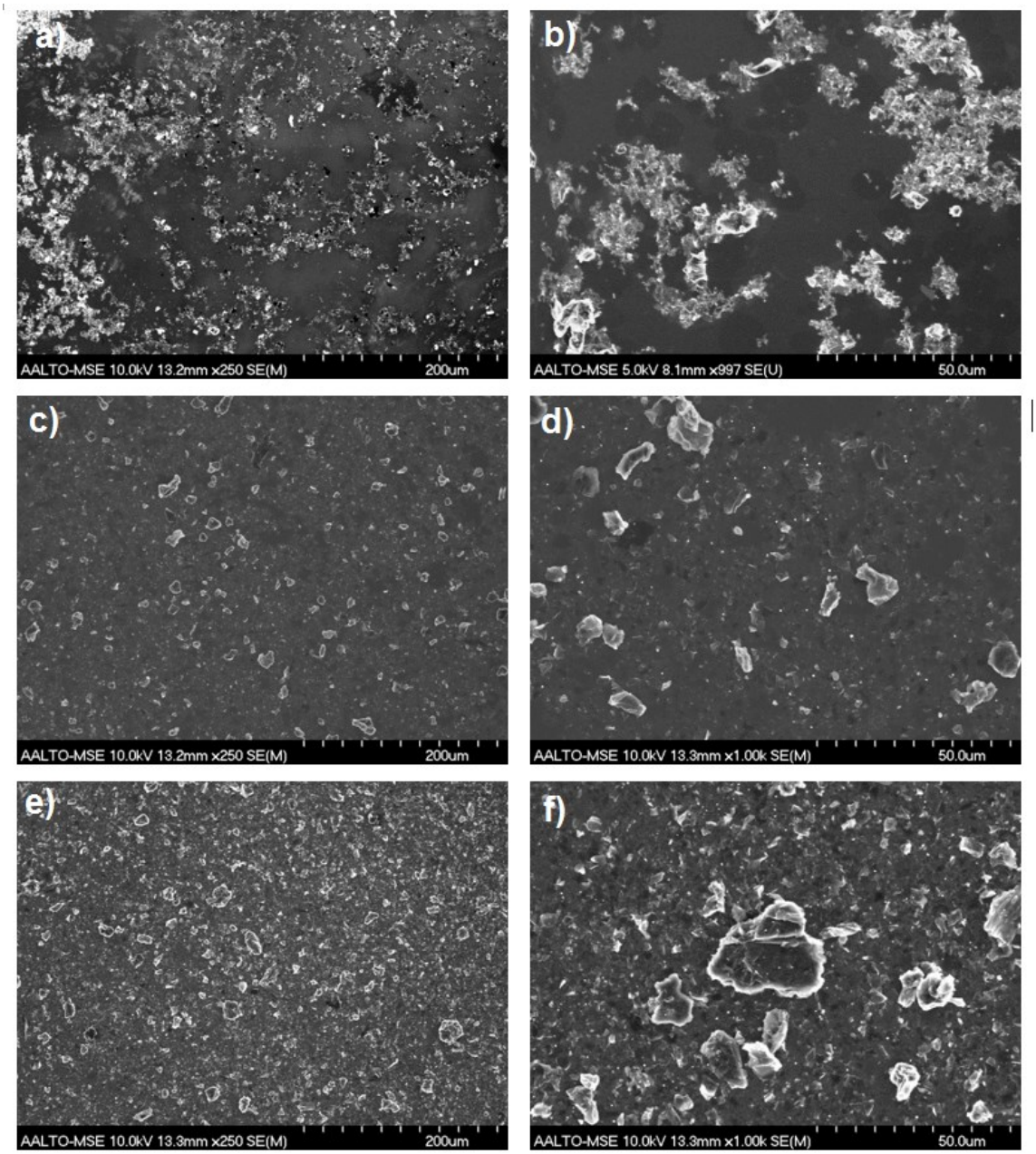

Figure 18. SEM images of a) and b) rGO-1, c) and d) rGO-3 as well as e) and f) rGO-5 electrodes.

The coverage of all electrodes can be seen to be reasonably uniform over the electrode surface area. It is, however, clear that the ta-C is only partially covered in the case of the rGO-1 electrode, while the rGO-3 and rGO-5 electrodes are fully covered by rGO. In the case of the rGO-3 electrode spots, which have very little rGO can also be observed. Such sites were not observed on the rGO-5 electrode. Moreover, large agglomerates several μm in size can be seen on all rGO modified electrodes. The amount of such agglomerates also clearly become more abundant with addition of rGO.

The partial coverage of the ta-C, especially with the rGO-1 electrode leads to two different exposed electrode materials. This can lead to problems if redox reactions occur at different potential on the two different materials. Therefore optimizing the system, by varying ta-C thickness and amount of rGO on the electrode is important for optimal performance.

At larger magnifications stacked rGO sheets with basal planes of several μm in size can be seen. The stacking also indicates incomplete exfoliation or stacking, subsequent to the reduction step, of the rGO sheets. Significant stacking also likely occurs during drying of the rGO solution. Figure 19 a) and b) show graphene nanoflakes with basal planes aligned parallel to the electrode surface. Nevertheless edge planes can be seen, especially around the edges of the particles. In Figure 19 c) and d) the edges of such graphene flakes are shown. The edge planes can clearly be seen at these magnifications. Additional information about stacking and number of graphene layers in the rGO flakes would require transmission electron microscopy (TEM).

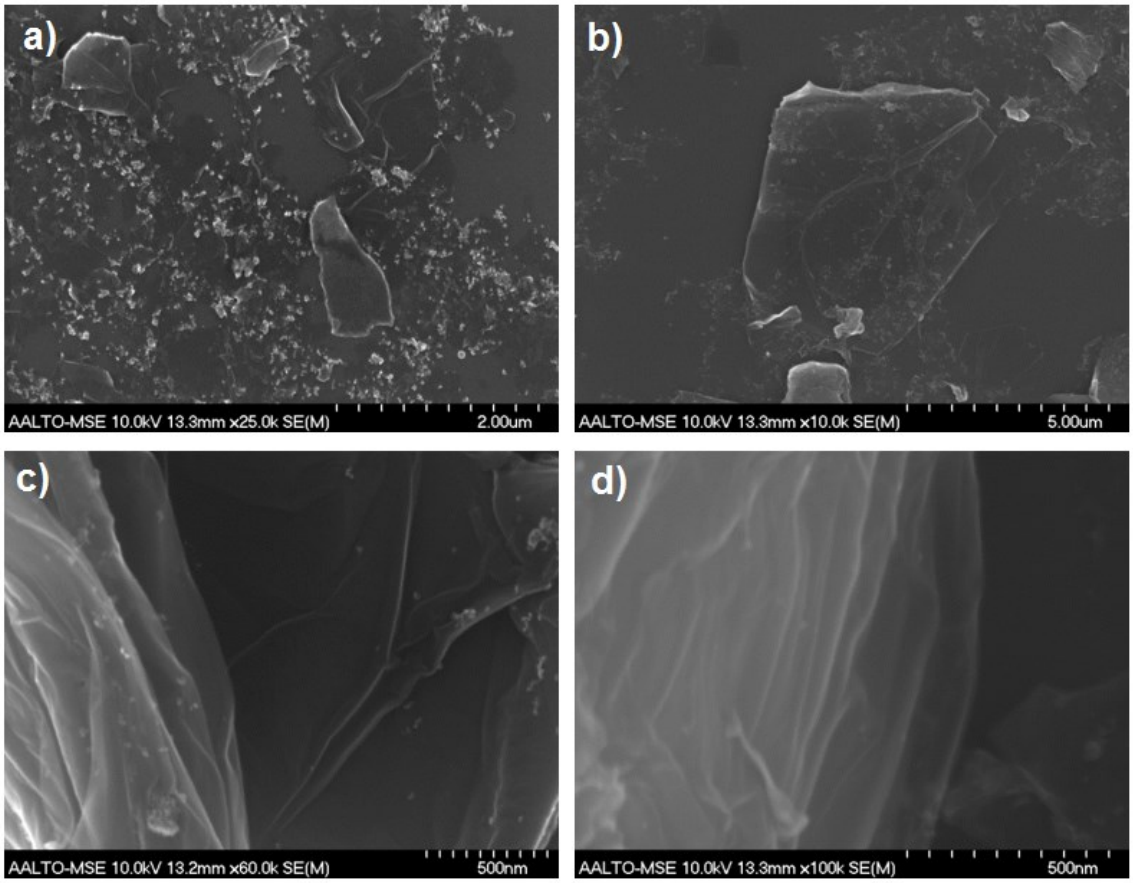

Figure 19. SEM image of a) and b) graphene nanoflakes with large exposed basal planes and c) and d) large magnification images of rGO flakes.

4.3.2 Raman spectroscopy

The bonding configuration of rGO was studied with Raman spectroscopy. For this a separate rGO sample was prepared by drop casting of one 40 µl drop on p-type (100) Si wafer.

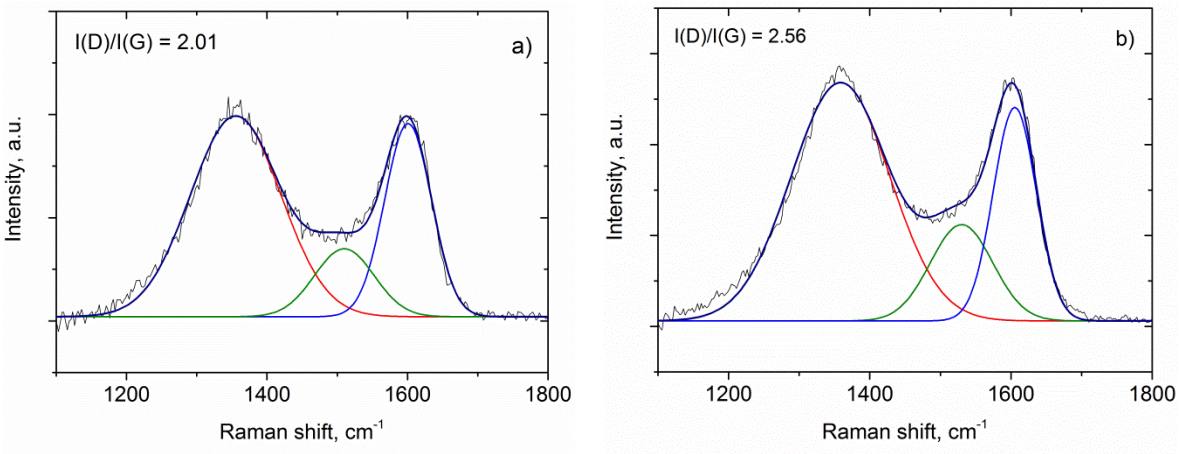

Figure 20. Raman spectrum of a) GO and b) rGO.

The Raman spectrum of pristine graphite is known to display only a prominent G peak at 1581 cm^{-1}. The Raman spectrum of rGO shows both G and D bands centered at 1605 and 1355 cm^{-1}, respectively. The I(D)/I(G) values of 2.01 and 2.56 for GO and rGO, respectively were found. The D peak is a measure of the disorder and defects in the graphene. The Raman spectra shown here are close to what has been reported previously in literature [77].

4.3.3 FT-IR spectroscopy

Chemically reduced graphene oxide is known to have oxygen containing functionalities. The functional groups of the rGO were characterized by FT-IR spectroscopy. Samples with 1, 3, and 5 drops of rGO were subjected to analysis both in the as deposited reduced form and after treatment with 10 M HNO_3. Figure 21 shows the FT-IR spectra for a) the GO as well as the rGO samples and b) the nitric acid treated samples.

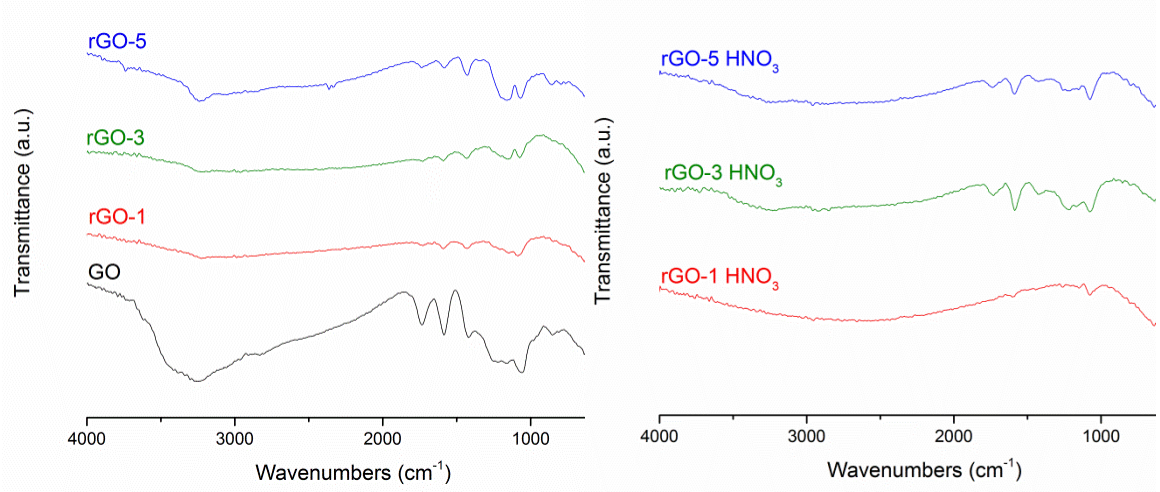

Figure 21. FT-IR spectra of a) GO and rGO-1, rGO-3 and rGO-5 and b) the NHO_3 treated electrodes.

The GO shows clear peaks related to oxygen containing functionalities, such as C = O stretching vibration peak at 1736 cm^{-1}, the vibration and stretching of O–H at 3395 cm^{-1} and 1410 cm^{-1}, respectively, the C–O (epoxy) stretching at 1227 cm^{-1}, as well as C–O (alkoxy) stretching at 1059 cm^{-1}. The rGO samples showed significant decrease in the intensity of all these peaks after reduction. Some residual oxygen containing groups were, however, detected. Small peaks for hydroxyl, carbonyl, epoxy and alkoxy groups were detected. The intensity of these peaks also increased with increasing amount of rGO as expected. The nitric acid treatment increased the intensity of all peaks related to oxygen containing functionalities of all rGO samples. The largest relative increase was observed for the rGO-3 sample. The SEM analysis showed that the rGO layer is fairly continuous, but at the same time porous and rough. This likely leads to acid exposure of a larger surface area and therefore a larger degree of functionalization, as compared to rGO-1 and rGO-5. It should be noted here that the FT-IR spectroscopy is more a qualitative than a quantitative analysis method. Therefore it is best to combine it with other, preferably surface sensitive techniques, such as X-ray photoelectron spectroscopy (XPS) or X-ray absorption spectroscopy (XAS) to obtain best possible results. To better understand the role of the oxygen containing surface functional groups more extensive characterization of surface chemistry would be required.

4.3.4 Cyclic voltammetry

4.3.4.1 Water window and double layer capacitance

The electrochemical behavior of the reduced graphene oxide modified ta-C electrodes was studied with cyclic voltammetry in PBS and 0.15 M H_2SO_4 solutions. The oxygen groups present in graphene oxide materials are known to be electroactive, and electrochemical reactions may occur when the rGO is cycled in relatively small potential ranges. Reduction of GO by cycling in a potential window of -1V to +1V (vs. Ag/AgCl) has been reported by Shao and coworkers [82]. They found that cycling in this window results in partial reduction of the GO and caused a stable redox couple to appear. Due to these electroactive oxygen containing groups known to be present in rGO the electrodes were cycled in different potential windows. Figure 22 shows the cyclic voltammograms of the rGO electrodes in a) sulfuric acid and b) PBS solution with cycling rate of 400 mV/s.

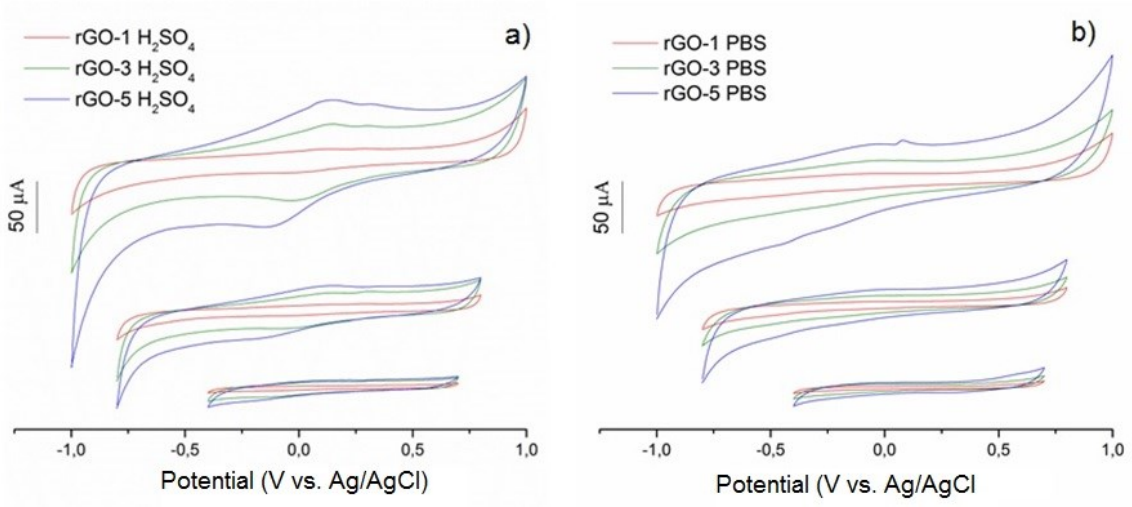

Figure 22. Cyclic voltammograms of rGO-modified electrodes in a) 0.15 M sulfuric acid and b) PBS solution in different potential windows.

In both sulfuric acid and PBS solution the capacitive current grows with addition of rGO. The rGO electrodes are relatively stable in the smallest potential range of -0.4 V to 0.7 V. In the H_2SO_4 solution the appearance of redox peaks can, however, already be observed in this small window, whereas no such peaks were observed in PBS. The cycling in larger potential windows also caused a redox couple to appear at approximately the same potential where DA undergoes oxidation and reduction. The activation of this redox couple appears

to be irreversible, and after activation in a large window the faradic peaks can be observed even if the potential window is decreased. Zhou et al. [86] found that the potential needed to realize reduction of GO is dependent on the electrolyte solution pH, and that low pH values favors the reduction of GO. Consequently they proposed that H^+ ions participate in the reaction. This finding is supported by the fact that the currents related to the redox couple are significantly larger in the mild sulfuric acid as compared to the PBS solution. As can be seen in Figure 22 by the absence of a flat region especially in larger potential windows, the faradic contribution to the measured current is considerable.

4.3.4.2 Ferrocenemethanol

The outer-sphere redox couple of ferrocene was used to probe the modified electrodes. Figure 23 shows the cyclic voltammogram of the rGO modified electrodes in 1 mM FcMeOH with cycling rates of a) 50 mV/s and b) 400 mV/s. Based on these voltammograms ΔE_p values were determined for each electrode. The values are presented in Table 6.

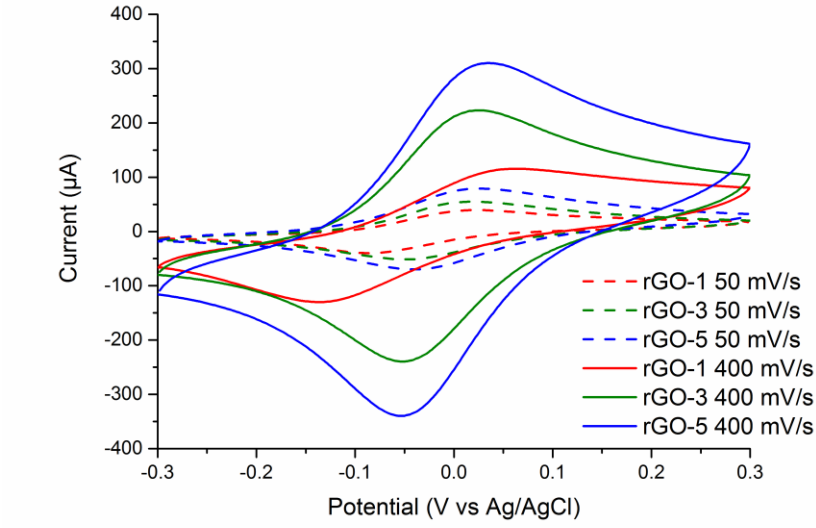

Figure 23. Cyclic voltammogram of rGO modified electrodes in 1 mM FcMeOH redox couple with 50 and 400 mV/s.

Table 6. Separation of oxidation and reduction peak potentials ΔE_p in the FcMeOH system for rGO modified electrodes.

Electrode	ΔEp Uncorrected [mV]		ΔE_p IR-corrected (80% Ru) [mV]	
	50 mV/s	400 mV/s	50 mV/s	400 mV/s
rGO-1	86	146	85	144
rGO-3	66	76	65	72
rGO-5	64	90	64	83

In systems with reversible one electron transfer the peak separation is 59 mV and is independent of the applied sweep rate. The Ti/ta-C bilayer electrode was determined to show quasireversible electron transfer, with low ΔE_p values of 61 and 70 mV, at cycling rates of 50 and 400 mV/s, respectively. The rGO-1 electrode shows slower electron transfer, at both sweep rates as compared to the unmodified electrode. This is likely caused by large exposed basal planes of the micron scale stacked rGO, which was clearly visible in the SEM images (Figures 18 and 19). When the amount of rGO was increased, a decrease in ΔE_p was observed. At the cycling rate of 50 mV/s ΔE_p values of 65 and 64 mV were observed for the rGO-3 and rGO-5 electrodes, respectively. An increase in the sweep rate to 400 mV/s caused an increase in the peak potential separation to values of 72 and 83 mV for the rGO-3 and rGO-5 electrodes, respectively. The observed behavior for all electrodes is quasireverisble. All with the exception of the rGO-1 electrode, show relatively high rates of electron transfer with the FcMeOH redox couple. The rGO-3 electrode showed the smallest increase in ΔE_p, as a result of increased sweep rate, and therefore based on these results shows the fastest electron transfer. The peak currents for the all the rGO modified electrodes are clearly larger than that of the unmodified electrodes, indicating larger active electrode area. The peak current ratio also does not deviate markedly from unity for any of the applied electrodes.

The FcMeOH redox couple is generally accepted to be an outer-sphere system and fairly insensitive to the surface of the electrode. It should, however, be noted that adsorption of FcMeOH to graphene has been reported [65]. For this reason further probing with other outer-sphere redox couples might be needed. During these experiments no significant

change in the rates of electron transfer was, however, observed with repeated measurements with the same electrodes. The retarded heterogeneous electron transfer kinetics observed for the partially covered rGO modified electrode highlights the importance of stacking and coverage of the rGO. It further shows that, contrary to what is commonly reported in literature, any addition of graphene or rGO cannot always be assumed to improve the electrode performance, at least when it comes to rates of heterogeneous electron transfer of outer sphere redox couples. Brownson et al. [13] reported similar results with HOPG electrodes partially covered by graphene monolayer flakes. They found that addition of graphene could either increase or decrease electrochemical reversibility of outer sphere systems, depending on the alignment and layering of the graphene on the electrode. Lounasvuori et al. [87] modified BDD electrodes with graphene nanoflakes (GNF) without any deterioration of heterogeneous electron transfer with the FcMeOH system. It is possible that the increased stacking observed for the rGO-3 and rGO-5 electrodes increase the amount of surface active sites for heteroelectron transfer. Brownson et al. [13] reported similar findings on a HOPG electrode.

4.3.4.3 Sensitivity towards dopamine

The sensitivity of the rGO modified electrode towards DA was determined with CV. As was shown in Figure 22, cycling of rGO in large potential windows leads to significant increase in the capacitive current. As small capacitive currents and absence of electrode surface redox couples are desired here, a small potential window of -0.4 V to 0.7 V was chosen for the measurements. Figures 24–26 show the results from the CV measurements in DA solution for a) rGO modified electrods and b) nitric acid treated rGO electrodes, with concentrations ranging from 100 nM to 10 µM.

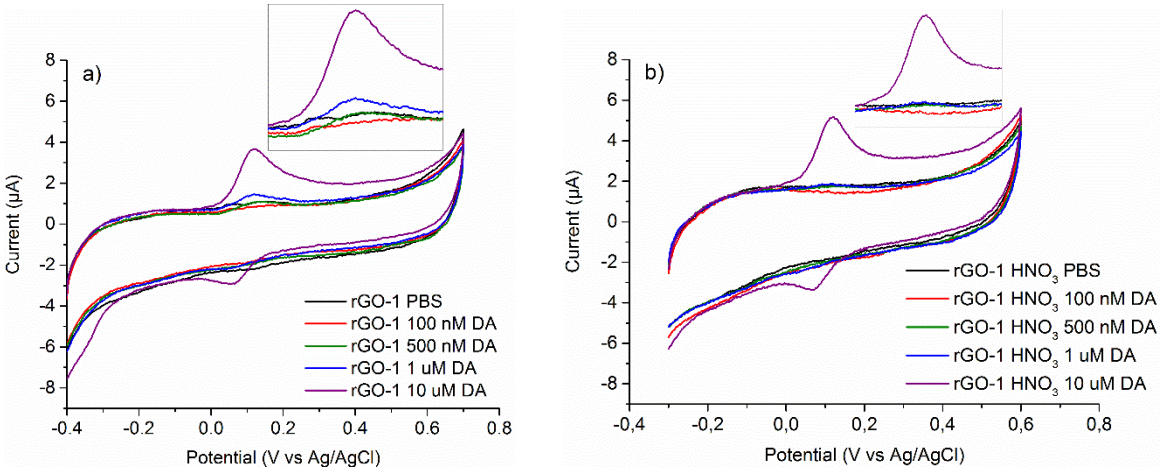

Figure 24. Cyclic voltammogram of a) rGO-1 and b) nitric acid treated rGO-1 electrodes in DA solutions with concentrations from 0.1 to 10 µM at a cycling rate of 50 mV/s.

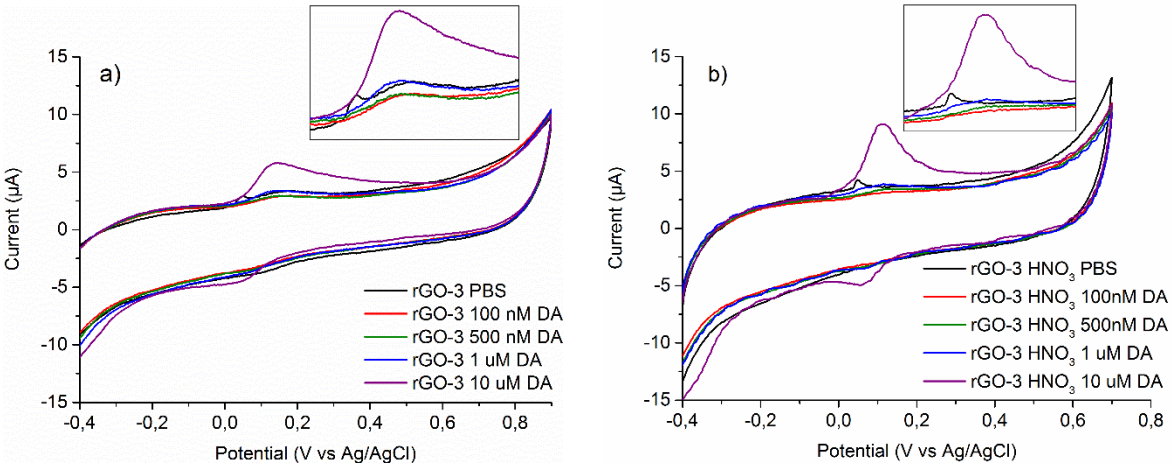

Figure 25. Cyclic voltammogram of a) rGO-3 and b) nitric acid treated rGO-3 electrodes in DA solutions with concentrations from 0.1 to 10 µM at a cycling rate of 50 mV/s.

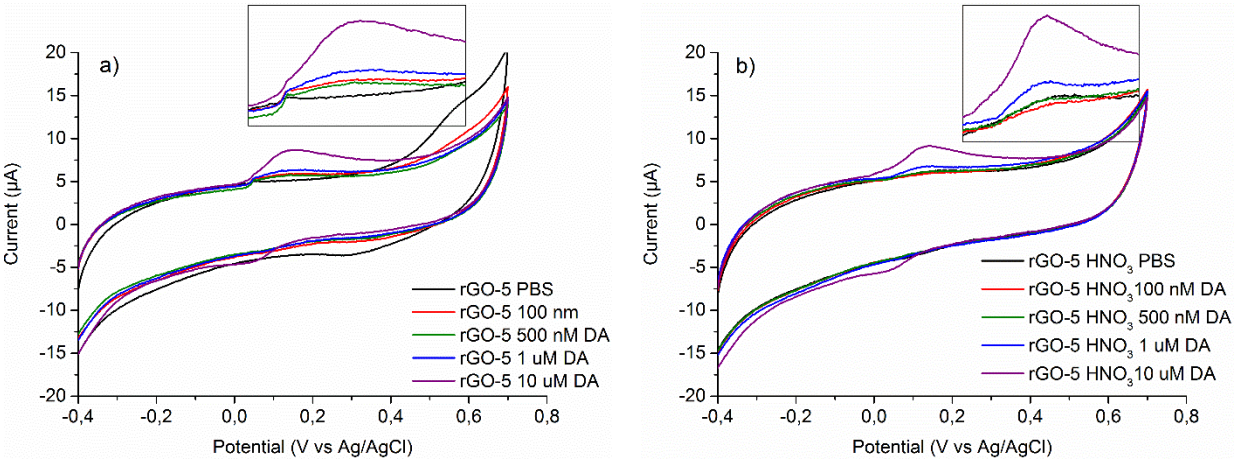

Figure 26. Cyclic voltammogram of a) rGO-3 and b) nitric acid treated rGO-3 electrodes in DA solutions with concentrations from 0.1 to 10 µM at a cycling rate of 50 mV/s.

The rGO-1 electrode shows a first small peak in the 500 nM DA solution, increasing the sensitivity by one order of magnitude as compared to the unmodified Ti/ta-C bilayer electrode. With the rGO-3 and rGO-5 electrodes on the other hand the first peaks were observed in 1 μM. In addition at low concentrations the peaks are sharper and better defined for the rGO-1 electrode as compared to the rGO-3 and rGO-5 electrodes. This is likely due to larger distribution of different active sites on the rGO-3 and rGO-5 electrodes. The nitric acid treatment showed a clear improvement in the performance of the rGO-3 electrode. The effect was significantly smaller for the rGO-1 and rGO-5 electrodes. As can be observed from Figures 24–26, a large change in the current can be observed with addition of DA at concentrations below the detection limit of the electrodes. In addition the blank PBS current is larger than that of 100 nm DA. More measurements are required to show if this is caused by drift in background current, due to passivation of the electrode or if the electrode can actually detect the changes in the EDL, with addition of DA. It should be noted here that for in vivo detection of DA the extracellular fluid will always contain some DA.

By calculating the sensitivity of the electrodes (μA/mM), limits of detection could be calculated according to the procedure given in [14]. With such methods detection limits as low as 1.26 nM for DA have been reported with MWCNT. [14] Moreover detection limits of 50 nM for CNFs [41], 90 nM for EPPG [88] and 170 nM for graphene [16] have been reported. The 500 nM detection limit achieved here is an actual measured increase in current with addition of DA and is sufficiently low for detection of DA transients in vivo. Most other works utilize the more sensitive differential pulse voltammetry (DPV) and the results presented here are among the best ever reported for CV measurements.

Table 7 shows the linear equations and fits of peak current as function of DA concentration in ranges 0.1–10 μM and 10–1000 μM. The best fit was obtained with the concentration range of 0.1 μM to 10 μM. The poor fit over the full range suggests two linear ranges for DA with the rGO electrodes.

Table 7. Linear fits of oxidation peak current as function of DA concentration in DA concentration range of 0.1 to 10 µM.

Electrode	Liner fit equation 0.1–10 µM	R^2
rGO-1	$Ip_a = 0.270 \cdot C_{DA} + 0.993$	0.9834
rGO-1 HNO_3	$Ip_a = 0.365 \cdot C_{DA} + 1.510$	0.9975
rGO-3	$Ip_a = 0.383 \cdot C_{DA} + 2.857$	0.9966
rGO-3 HNO_3	$Ip_a = 0.596 \cdot C_{DA} + 3.158$	0.9994
rGO-5	$Ip_a = 0.270 \cdot C_{DA} + 5.808$	0.9888
rGO-5 HNO_3	$Ip_a = 0.340 \cdot C_{DA} + 6.100$	0.9816

Similar results with two linear ranges for DA were presented by Shang et al. [16] with CVD graphene nanoflake film electrodes. They found linear ranges of 1 to 50 µM and 50–100 µM. For the higher linear concentration range only two data points are available. Measurements at additional concentrations above 50 µM are required to confirm linear current response in this high concentration region. It is however worth mentioning that in vivo DA concentrations never exceeds 10 µM, making the linear range found more than adequate for in vivo detection of DA. The nitric acid treatment can also be seen to increase the current response for DA in this concentration range. The increase in the intercept for the current axis also indicates a small increase in capacitive current when the rGO electrodes are treated with nitric acid. The current response was also observed to grow.

The kinetics of the DA system was studied by determining the peak potential separation of the first oxidation and reduction peaks. Figures 27 and 28 show the voltammograms of the rGO electrodes and nitric acid treated rGO electrodes in 100 µM and 1 mM DA solutions, respectively.

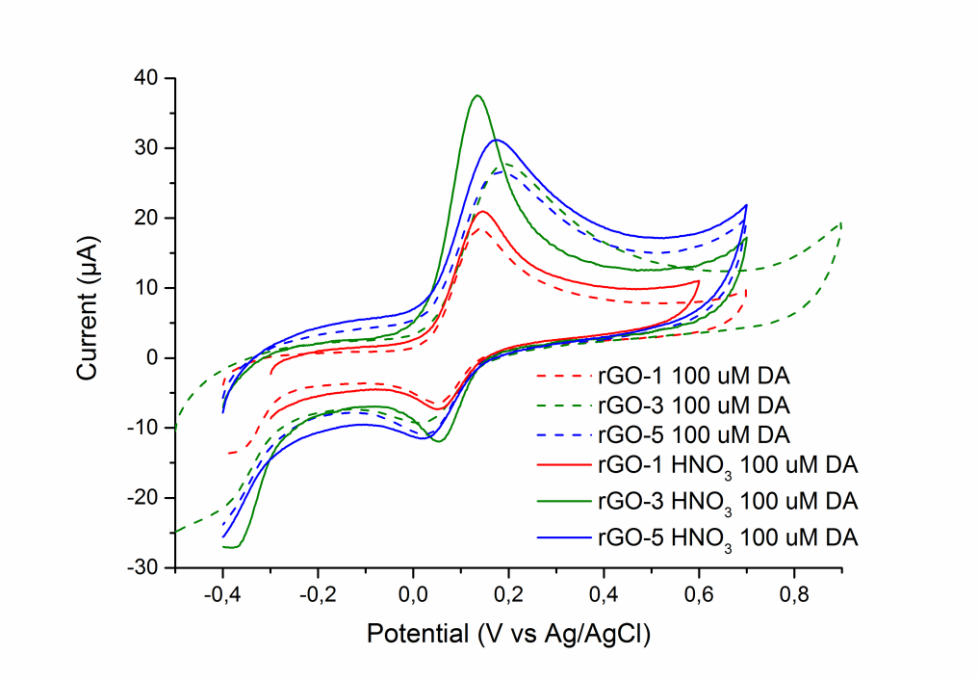

Figure 27. Cyclic voltammogram of the rGO and nitric acid treated rGO electrodes in 100 µM DA solutions with cycling rate of 50 mV/s.

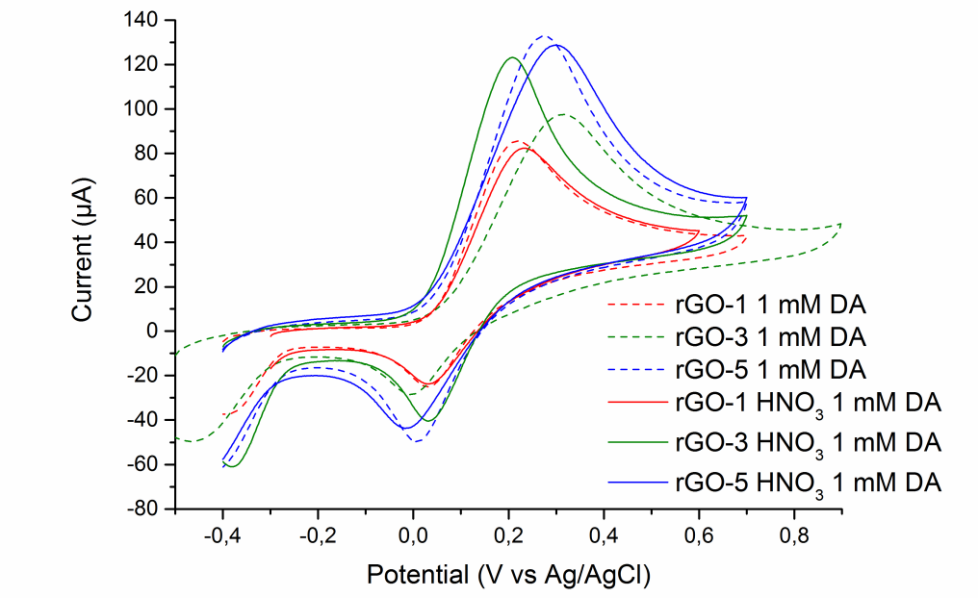

Figure 28. Cyclic voltammogram of the rGO and nitric acid treated rGO electrodes in 1 mM DA solutions with cycling rate of 50 mV/s.

A large shift can be observed in the oxidation peak potential of the rGO-3 electrode. The change is significantly smaller with the two other electrodes. At 100 µM DA concentration the peak current is larger for all nitric acid treated rGO electrodes. In the 1 mM DA solution difference is negligible, except for the rGO-3 electrode. The peak potential separation values for the rGO electrodes are shown in the Table 8.

Table 8. Peak potential separation ΔEp of the rGO electrodes in 10 µM, 100 µM and 1 mM DA solutions.

Electrode	Peak potential separation ΔE_p (mV)		
	10 µM	100 µM	1 mM
rGO-1	64	91	183
rGO-1 HNO3	56	93	252
rGO-3	102	173	295
rGO-3 HNO3	60	78	170
rGO-5	104	162	259
rGO-5 HNO3	82	156	308

The ΔE_p values were 422 mV for the ta-C electrode in 1 mM DA solution. All the rGO electrodes show significantly lower ΔE_p values, indicating faster electron transfer kinetics and a more reversible system. The ΔE_p values for the untreated and nitric acid treated rGO-1 were 64 mV and 56 mV, respectively at 10 µM DA concentration. These values grow to 91 and 93 mV when the concentration is increased to 100 µM and further increase to 183 and 252 mV at 1 mM DA concentration. The same trend of growing ΔE_p values with increasing DA concentrations can be observed for all rGO electrodes. The smallest ΔE_p values at 10 µM DA concentration for nitric acid treated the rGO-1 and rGO-3 electrodes were of 56 and 60 mV, respectively. This is indicative of reasonably high electron transfer, but does still not reach the ideal value of 29.8 mV for the two electron two proton transfer electro-oxidation reaction of DA.

The heterogeneous electron transfer rates as measured with the FcMeOH redox couple are not reflected in the DA measurements. The rGO-1 electrode actually showed a lower electron transfer constant compared to the unmodified ta-C electrode. Thus the lower

detection limit, significantly larger current response, and faster kinetics in the DA system compared to the ta-C electrode are proposed to be more dependent on surface properties than on the rates of electron transfer. This may be due to high amount of active sites which facilitate adsorption and electron transfer of DA on the rGO electrodes.

4.3.4.4 Selectivity towards dopamine in DA + AA systems

Measurement of endogenous DA includes the effect of interferents, such as ascorbic acid (AA), uric acid (UA) and serotonin. The levels of these interferents may be several orders of magnitude higher in extracellular fluid, compared to the biomolecule of interest [3]. To probe the selectivity towards DA measurements with DA in the presence of AA were carried out. To characterize the electrochemical behavior of AA on the rGO electrodes, measurements with only AA were first carried out. Figure 29 shows the cyclic voltammograms of the untreated rGO and the nitric acid treated rGO electrodes in 1 mM AA solution.

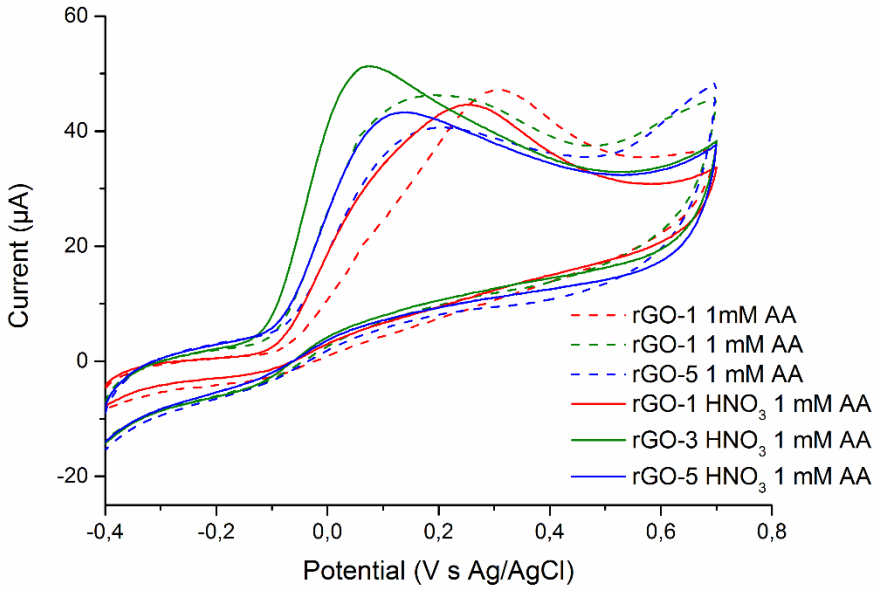

Figure 29. Cyclic voltammogram of untreated and nitric acid treated rGO electrodes in 1 mM AA solution with scan rate of 50 mV/s.

The oxidation of AA starts at a potential around –100 mV, but can be seen to continue at overpotentials. For this reason no sharp peaks were observed. Instead broad peaks with peak potentials much larger than –100 mV were observed. Nitric acid treatment shifted the

peak potentials of all rGO electrodes. Recently a similar shift in the AA oxidation peak was presented for CNT electrode [14]. In addition L-ascorbic acid has previously been used as a reducing agent for GO [80]. This indicates that chemical reactions between AA and oxygen containing functional groups on the electrode surface occur spontaneously in AA solutions. This likely explains the catalytic effect observed at the nitric acid treated electrodes. It should be noted that while there is a significant shift in the oxidation peak potential of AA at the nitric acid treated rGO electrodes the oxidation potential of DA is not significantly affected. It is, however, unclear if this effect is temporary, and if the oxygen containing groups that provide catalytic sites for AA oxidation are consumed when AA is oxidized.

The measured oxidation peak potentials of AA and DA are presented in Table 9. The treated electrodes also produced sharper peaks, with the exception of the rGO-1 electrode for which a stronger shoulder and a broader peak appeared. The largest shift was observed for the rGO-3 electrode, resulting in a peak potential difference of 134 mV. Figures 30 and 31 show the cyclic voltammograms of the a) untreated and nitric acid treated b) rGO-3 and rGO-5 electrodes, respectively.

Table 9. Oxidation peak potential of untreated and nitric acid treated rGO electrodes in 1 mM AA and 1 mM DA with scan rate of 50 mV/s.

Electrode	AA oxidation potential (mV)	DA oxidation potential (mV)
rGO-1	254	183
rGO-1 HNO_3	310	252
rGO-3	214	295
rGO-3 HNO_3	74	170
rGO-5	207	259
rGO-5 HNO_3	140	308

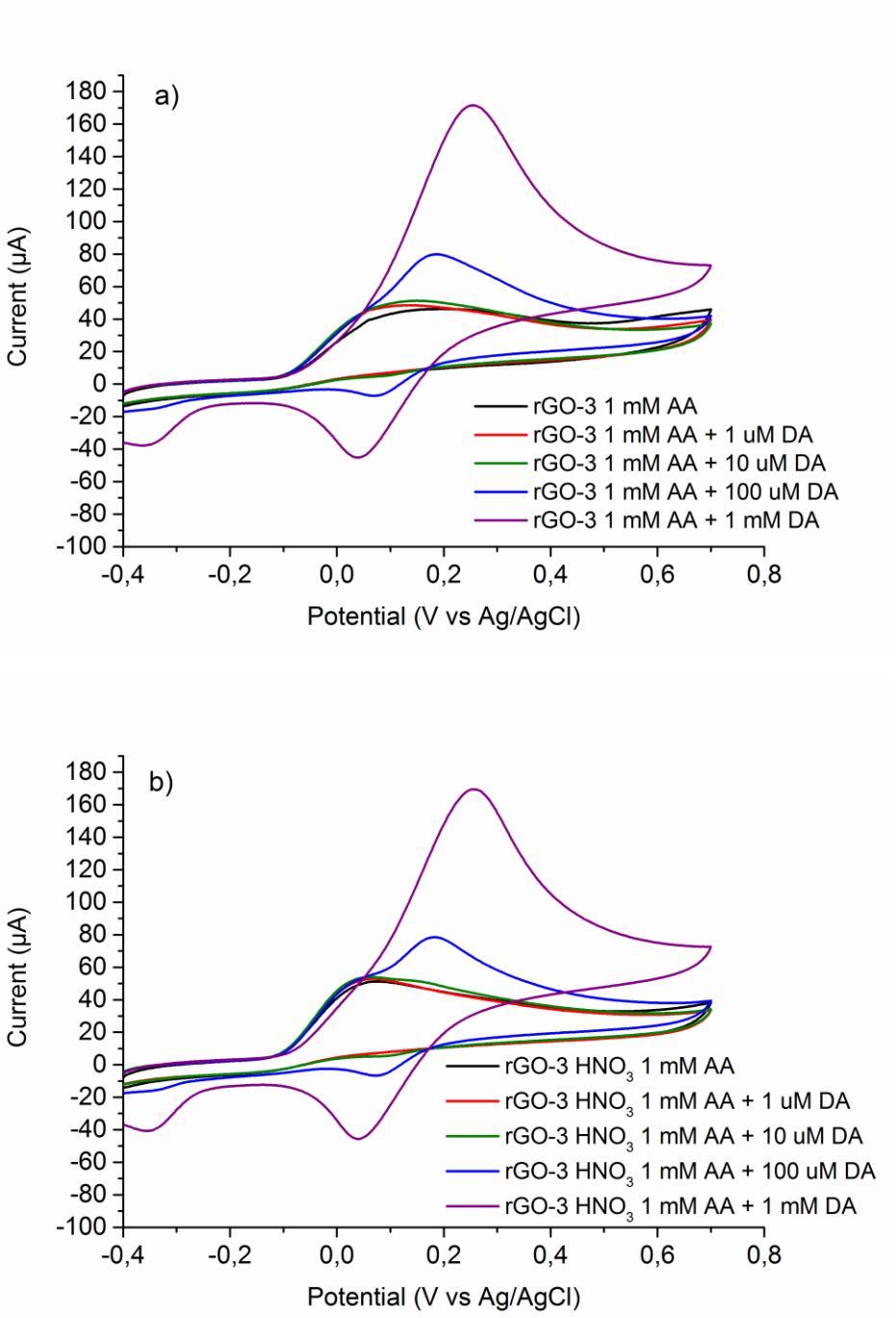

Figure 30. Cyclic voltammogram of a) untreated and b) nitric acid treated rGO electrodes in varying DA concentration in the presence of 1 mM AA with scan rate of 50 mV/s.

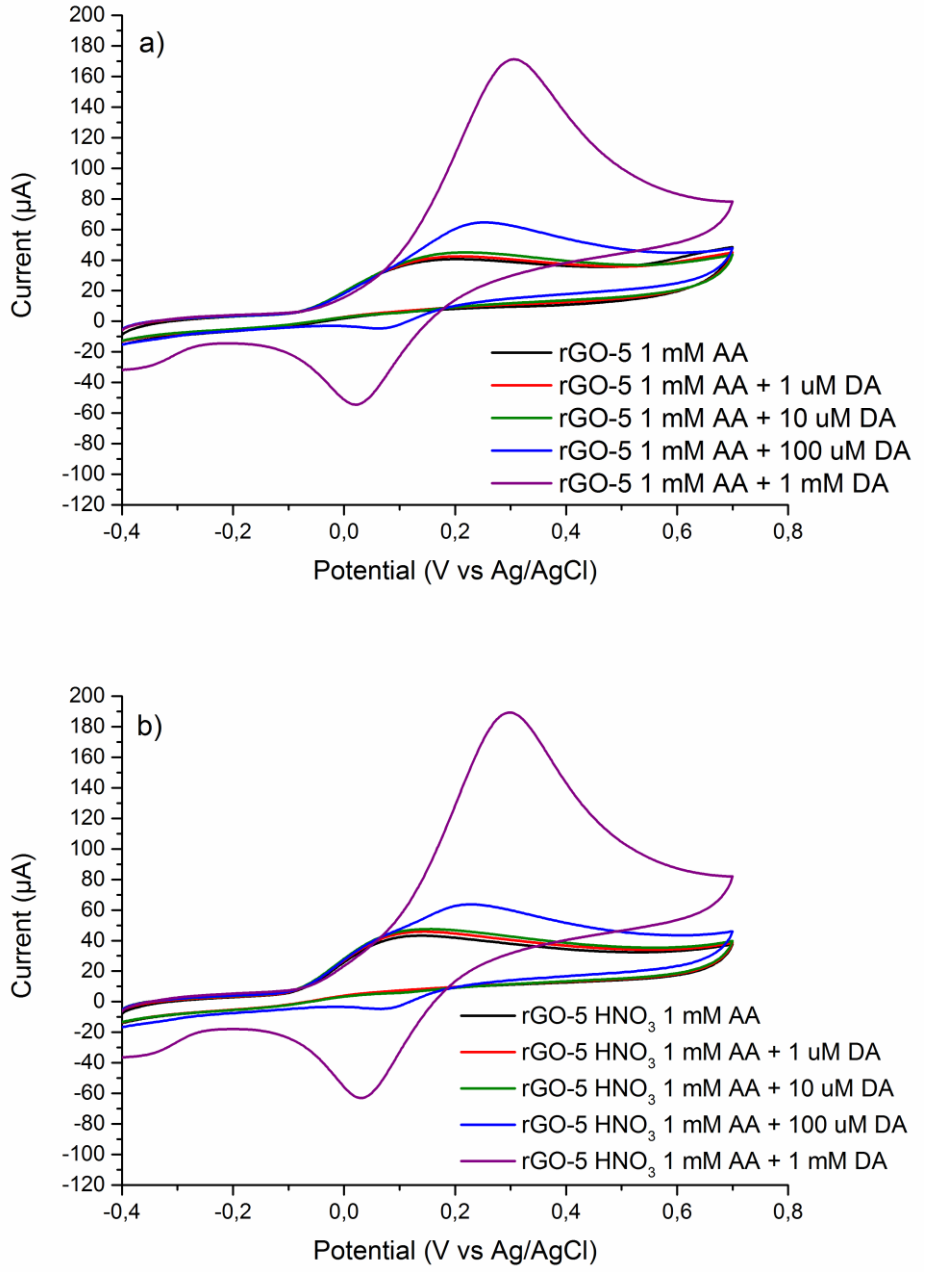

Figure 31. Cyclic voltammogram of a) untreated and b) nitric acid treated rGO electrodes in varying DA concentration in the presence of 1 mM AA with scan rate of 50 mV/s.

The rGO-3 and rGO-5 electrodes were also the ones that showed the highest amount of oxygen containing groups in the FT-IR characterization. The rGO-3 electrode showed the largest relative increase in oxygen containing groups. For both the electrodes rGO-3 and rGO-5 the first DA concentration at, which a clear peak can be observed is 10 µM. This is

problematic for selective in vivo detection of DA by cyclic voltammtery. The currents observed in these measurements are, however, relatively large and uncompensated resistance may therefore have caused significant IR-drop. The problem could possibly be alleviated by reducing the area of the electrodes. Moreover, in vivo measurements require the use of microelectrodes, in which case mass transfer of analyte is enhanced and the IR-drop caused by uncompensated resistance is significantly reduced.

High selectivity towards DA has previously been reported for various types of graphene electrodes. Shang et al. [16] achieved a peak potential separation of 181 mV between the AA and DA oxidation peaks with a CVD multilayer graphene nanoflake electrode. The AA, however, also showed a significant diffusive tail and CV with the ternary system containing AA, DA and UA was carried out at a scan rate of 100 mV/s. As was shown in Figure 15 the peak current is directly correlated to the square root of scan rate, and higher scan rate will therefore produce larger and possibly better resolved peaks.

The SEM images presented above shoved that the rGO-1 electrode had large areas of exposed ta-C. The rGO-3 also showed small areas of exposed ta-C. In addition the rGO layer especially on the rGO-3, but also likely on rGO-5 electrodes, is relatively porous. The exposed ta-C is expected to significantly contribute to the measured current, as AA will produce a very wide peak with oxidation starting at around 0 V and peak current maximum at 344 mV on the ta-C electrode.

The rGO-3 electrode was found to show the highest selectivity in measurements with solutions containing 1 mM AA and DA concentrations ranging from 1 μM to 1 mM. In addition it was found that a 5 min treatment with concentrated 10 M HNO_3 further increased selectivity, shifting the oxidation peak of AA toward more negative potentials. This phenomenon has also been observed with CNT electrodes [14]. The selectivity is an important advantage of the rGO modified electrode, as the plain ta-C electrode cannot distinguish between DA and AA, and shows voltammetric peak overlap. A relatively large amount of rGO seems to be required in order to achieve good selectivity towards DA. Based on the these cyclic voltammetry measurements the amount of rGO seems to affect the electrochemical performance of the electrodes in the presence of AA.

5 Summary

Cyclic voltammetry experiments were carried out in sulfuric acid, PBS solution and DA solutions of varying concentrations to evaluate the performance of ta-C and rGO modified ta-C in biosensing applications. It was shown that by controlling the thickness of ultrathin ta-C top layer it is possible to influence electron transfer properties of the outer sphere FcMeOH system. Electron transfer was improved by reducing ta-C thickness, while only small decrease in water window and capacitive background current were observed. At thicknesses of 4 nm and below electroactivity of the underlying Ti was observed, resulting in significant changes in background current with continued cycling. An increase in background current and decrease in water window as well as heterogeneous electron transfer was also observed. The thickness did not influence the sensitivity towards dopamine, as the same detection limit of 5 µM was obtained for each ta-C electrode. This detection limit of the ta-C electrodes is not low enough for in vivo DA sensing applications. Moreover, the electrode exhibited poor selectivity towards DA in a solution with ascorbic acid as an interferent. Owing to its chemical inertness, relatively low capacitive current, wide water window, and patternability, the Ti/ta-C bilayer electrode, however, presents an excellent mediating base layer for modification.

By modifying the Ti/ta-C electrode with rGO one order of magnitude lower detection limit of 500 nM for DA was achieved. Modification with one drop rGO solution was found to retard the heterogeneous electron transfer in an outer sphere system. The rGO-3 and rGO-5 electrodes with more rGO showed improved or comparable electron transfer rates. The electron transfer rates in the outer sphere system did not significantly affect detection of DA and in fact the rGO-1 electrode exhibited the lowest detection limit of all rGO modified electrodes. The detection limit of both rGO-3 and rGO-5 electrodes was 1 µM. The rGO-1 electrode, however, showed poor selectivity towards DA, and AA and DA peaks were not distinguishable. The rGO-3 and rGO-5 electrodes on the other hand produced separate peaks for AA and DA, with differences in oxidation peak positions of 81 and 52 mV, respectively.

In addition HNO_3 treatments were carried out to for each rGO modified electrode, and were found to improve both sensitivity and selectivity towards DA. After nitric acid treatment

all rGO electrodes were able to detect 500 nM DA concentration, and showed linear current response in the range of 0.1-1000 μM. Moreover this treatment increased selectivity towards DA by shifting the AA oxidation peak to more negative values. The treatment, however, had only negligible effect on the rGO-1 electrode. For the rGO-3 and rGO-5 electrodes significantly larger oxidation peak potential separations of 96 and 168 mV, respectively, were achieved.

6 Conclusions

To the best knowledge of the author this is the first time that a ta-C electrode has been modified with rGO and applied in electrochemical detection of DA. The ta-C thickness of the Ti/ta-C bilayer electrode reported in earlier works has been optimized in terms of electron transfer properties. The optimum thickness for which ta-C prevents the passivation of the Ti/ta-C interface and facile heterogeneous electron transfer was observed, was found to be 7 nm. Owing to its electrochemical properties and CMOS compatibility this electrode is an ideal candidate for modification with rGO.

By combining the stability, good electron transfer properties and the reasonably low capacitive currents of the Ti/ta-C bilayer electrode with the more electrochemically active rGO, an electrode with substantially improved sensitivity and selectivity towards DA was achieved. This electrode also exhibited wide enough water window and sufficiently low capacitive background currents for electrochemical detection of DA. With the rGO modified electrodes a detection limit of 500 nM was achieved without data treatment. This detection limit is among the best ever reported. This result suggests that this electrode can be used to detect changes in DA concentrations below 1 µM concentrations by means of cyclic voltammetry. The rGO electrode shows great promise for real time in vivo detection of DA.

The results presented here also strongly suggest that the microstructure, amount and surface chemistry of the rGO electrodes play an important role in both sensitivity and the selectivity towards DA. The improvement in electrode performance subsequent to HNO_3 treatment highlights the importance of oxygen containing functional groups in electrochemical detection of DA. More work is required to fully understand the catalytic effect of these oxygen containing groups especially for the important interferent AA, but also for DA. Currently work is ongoing on more careful characterization of the surface chemistry and microstructure of the rGO electrodes. Moreover, the effect of cycling in large windows as well as anodic and cathodic treatments, on electrochemical performance should be studied in greater detail.

The ta-C/rGO hybrid material shows promise as an electrode material for in vivo detection of DA. The ability to selectively detect changes in currents at DA concentrations known to

correspond to DA transients in the extracellular fluid in the brain is a sought after property. Here the first steps towards realizing such an electrode have been taken. A number of issues, including long term stability, drifts in background currents and biofouling, however, still need to be resolved, before this electrode can be reliably applied for in vivo measurements. Another issue is the fabrication of ta-C-graphene microelectrode with similar electrochemical properties. In addition the sensitivity and selectivity also need to be further optimized.

References

1. Bear, M.F., Connors, B.W. and Paradiso, M.A. *Neuroscience: Exploring the Brain*. Philadelphia, PA, Lippincott Williams & Wilkins, cop. 2007.
2. Jackowska, K., and Krysinski, P. (2013). New trends in the electrochemical sensing of dopamine. *Analytical and bioanalytical chemistry*, 2013, vol. 405. pp. 3753-3771.
3. Robinson, D.L., Hermans, A., Seipel, A.T. and Wightman, R.M. Monitoring Rapid Chemical Communication in the Brain. *Chemical Reviews*, 2008, vol. 108, pp. 2554-2584.
4. Robinson, D.L., Venton, B.J., Heien, M.L.A.V. and Wightman, R.M. Detecting Subsecond Dopamine Release with Fast-Scan Cyclic Voltammetry in Vivo. *Clinical Chemistry*, 2003, vol. 49, pp. 1763-1773.
5. Sofuoglu, M., and Sewell, R. A. REVIEW: Norepinephrine and stimulant addiction. *Addiction biology*, 2009, vol. 14, pp. 119-129.
6. Venton, B. J., and Wightman, R. M. Psychoanalytical electrochemistry: dopamine and behavior. *Analytical Chemistry*, 2003, vol. 75, pp. 414 A-421 A.
7. Gustavsson, A., Svensson, M., Jacobi, F., Allgulander, C., Alonso, J., Beghi, E., ... and CDBE2010 Study Group. Cost of disorders of the brain in Europe 2010. *European Neuropsychopharmacology*, 2011, vol. 21, pp. 718-779.
8. Zeng, A., Neto, V. F., Gracio, J. J., and Fan, Q. H. Diamond-like carbon (DLC) films as electrochemical electrodes. *Diamond and Related Materials*, 2014, vol. 43, pp. 12-22.
9. Laurila, T., Rautiainen, A., Sintonen, S., Jiang, H., Kaivosoja, E., and Koskinen, J. Diamond-like carbon (DLC) thin film bioelectrodes: Effect of thermal post-treatments and the use of Ti adhesion layer. *Materials Science and Engineering: C*, 2014, vol. 34, pp. 446-454.
10. Laurila, T., Protopopova, V., Rhode, S., Sainio, S., Palomäki, T., Moram, M., Feliu, J.M., and Koskinen, J. New electrochemically improved tetrahedral amorphous carbon films for biological applications. *Diamond and Related Materials*, 2014, vol. 49, pp. 62-71.

11. Pumera, M., Ambrosi, A., Bonanni, A., Chng, E. L. K., and Poh, H. L. Graphene for electrochemical sensing and biosensing. *TrAC Trends in Analytical Chemistry*, 2010, vol. 29(9), pp. 954-965.
12. Davies, T. J., Michael E. Hyde, and Richard G. Compton. Nanotrench arrays reveal insight into graphite electrochemistry. *Angewandte Chemie*, 2005, vol. 117, pp. 5251-5256.
13. Brownson, D. A., Munro, L. J., Kampouris, D. K., and Banks, C. E. Electrochemistry of graphene: not such a beneficial electrode material?. *Rsc Advances*, 2011, vol. 1, pp. 978-988.
14. Sainio, S., Palomäki, T., Rhode, S., Kauppila, M., Pitkänen, O., Selkälä, T., Toth, G., Moram, M., Kordas, K., Koskinen, J., and Laurila, T. Carbon nanotube (CNT) forest grown on diamond-like carbon (DLC) thin films significantly improves electrochemical sensitivity and selectivity towards dopamine. *Sensors and Actuators B: Chemical*, 2015, vol. 211, pp. 177-186.
15. Wang, Y., Li, Y., Tang, L., Lu, J., and Li, J. Application of graphene-modified electrode for selective detection of dopamine. *Electrochemistry Communications*, 2009, vol. 11, pp. 889-892.
16. Shang, N. G., Papakonstantinou, P., McMullan, M., Chu, M., Stamboulis, A., Potenza, A., Dhesi, S.S., and Marchetto, H. Catalyst-free efficient growth, orientation and biosensing properties of multilayer graphene nanoflake films with sharp edge planes. *Advanced functional materials*, 2008, vol. 18, pp. 3506-3514.
17. Yang, L., Liu, D., Huang, J., and You, T. Simultaneous determination of dopamine, ascorbic acid and uric acid at electrochemically reduced graphene oxide modified electrode. *Sensors and Actuators B: Chemical*, 2014, vol. 193, pp. 166-172.
18. Sheng, Z. H., Zheng, X. Q., Xu, J. Y., Bao, W. J., Wang, F. B., and Xia, X. H. Electrochemical sensor based on nitrogen doped graphene: simultaneous determination of ascorbic acid, dopamine and uric acid. Biosensors and Bioelectronics, 2012, vol. 34, pp. 125-131.
19. Bungay, P. M., Newton-Vinson, P., Isele, W., Garris, P. A., and Justice, J. B. Microdialysis of dopamine interpreted with quantitative model incorporating probe implantation trauma. *Journal of neurochemistry*, 2003, vol. 86, pp. 932-946.

20. Bard, A.J., Bard, A.J. and Faulkner, L.R. Electrochemical Methods: Fundamentals and Applications. New York (N.Y.), Wiley, 2000.
21. Adams, R. N., and Marsden, C. A. Electrochemical detection methods for monoamine measurements in vitro and in vivo. In Handbook of psychopharmacology (pp. 1-74). Springer US., 1982.
22. Compton, R.G. and Banks, C.E. Understanding Voltammetry. London, Imperial College Press, 2010.
23. Nicholson, R. S. Theory and Application of Cyclic Voltammetry for Measurement of Electrode Reaction Kinetics. *Analytical Chemistry*, 1965, vol. 37, pp. 1351-1355.
24. Corona-Avendaño, S., Alarcón-Angeles, G., Ramírez-Silva, M.T., Rosquete-Pina, G., Romero-Romo, M. and Palomar-Pardavé, M. On the electrochemistry of dopamine in aqueous solution. Part I: The role of [SDS] on the voltammetric behavior of dopamine on a carbon paste electrode. *Journal of Electroanalytical Chemistry*, 2007, vol. 609, pp. 17-26.
25. Wen, X., Jia, Y. and Liu, Z. Micellar effects on the electrochemistry of dopamine and its selective detection in the presence of ascorbic acid. *Talanta*, 1999, vol. 50, pp. 1027-1033.
26. Tse, D.C.S., McCreery, R.L. and Adams, R.N. Potential oxidative pathways of brain catecholamines. *Journal of Medicinal Chemistry*, 1976, vol. 19, pp. 37-40.
27. Li, Y., Liu, M., Xiang, C., Xie, Q. and Yao, S. Electrochemical quartz crystal microbalance study on growth and property of the polymer deposit at gold electrodes during oxidation of dopamine in aqueous solutions. *Thin Solid Films*, 2006, vol. 497, pp. 270-278.
28. Domenech, A., Garcia, H., Domenech-Carbo, M.T. and Galletero, M.S. 2,4,6-Triphenylpyrylium Ion Encapsulated into Zeolite Y as a Selective Electrode for the Electrochemical Determination of Dopamine in the Presence of Ascorbic Acid. *Analytical Chemistry*, 2002, vol. 74, pp. 562-569
29. DuVall, S.H. and McCreery, R.L. Self-catalysis by Catechols and Quinones during Heterogeneous Electron Transfer at Carbon Electrodes. *Journal of the American Chemical Society*, 2000, vol. 122, pp. 6759-6764.

30. DuVall, S.H. and McCreery, R.L. Control of Catechol and Hydroquinone Electron-Transfer Kinetics on Native and Modified Glassy Carbon Electrodes. *Analytical Chemistry*, 1999, vol. 71, pp. 4594-4602.
31. Bath, B.D., Michael, D.J., Trafton, B.J., Joseph, J.D., Runnels, P.L. and Wightman, R.M. Subsecond Adsorption and Desorption of Dopamine at Carbon-Fiber Microelectrodes. *Analytical Chemistry*, 2000, vol. 72, pp. 5994-6002.
32. Deinhammer, R. S., Ho, M., Anderegg, J. W., and Porter, M. D. Electrochemical oxidation of amine-containing compounds: a route to the surface modification of glassy carbon electrodes. *Langmuir*, 1994, vol. 10, pp. 1306-1313.
33. Nicholson, C., and Phillips, J. M. Ion diffusion modified by tortuosity and volume fraction in the extracellular microenvironment of the rat cerebellum. *The Journal of Physiology*, 1981, vol. 321, pp. 225-257.
34. Fornstedt, B., Rosengren, E., and Carlsson, A. Occurrence and distribution of 5-S-cysteinyl derivatives of dopamine, dopa and dopac in the brains of eight mammalian species. *Neuropharmacology*, 1986, vol. 25, pp. 451-454.
35. Stamford, J. A., Kruk, Z. L., and Millar, J. Regional differences in extracellular ascorbic acid levels in the rat brain determined by high speed cyclic voltammetry. *Brain research*, 1984, vol. 299, pp. 289-295.
36. O'Neill, R. D., and Lowry, J. P. On the significance of brain extracellular uric acid detected with in-vivo monitoring techniques: a review. *Behavioural brain research*, 1995, vol. 71, pp. 33-49.
37. Ernst, H., and Knoll, M. Electrochemical characterisation of uric acid and ascorbic acid at a platinum electrode. *Analytica chimica acta*, 2001, vol. 449, pp. 129-134.
38. Wester, P., Hardy, J. A., Marcusson, J., Nyberg, P., and Winblad, B. Serotonin concentrations in normal aging human brains: relation to serotonin receptors. *Neurobiology of aging*, 1984, vol. 5, pp. 199-203.
39. Mefford, I., Oke, A., Keller, R., Adams, R. N., and Jonsson, G. Epinephrine distribution in human brain. *Neuroscience letters*, 1978, vol. 9, pp. 227-231.
40. Grünewald, R. A. Ascorbic acid in the brain. *Brain Research Reviews*, 1993, vol. 18, pp. 123-133.

41. Rand, E., Periyakaruppan, A., Tanaka, Z., Zhang, D. A., Marsh, M. P., Andrews, R. J., Lee, K. H, Chen, B. and Koehne, J. E. A carbon nanofiber based biosensor for simultaneous detection of dopamine and serotonin in the presence of ascorbicacid. *Biosensors and Bioelectronics*, 2013, vol. 42, pp. 434-438.
42. Ruiz, J. J., Aldaz, A., and Dominguez, M. Mechanism of L-ascorbic acid oxidation and dehydro-L-ascorbic acid reduction on a mercury electrode. I. Acid medium. *Canadian Journal of Chemistry*, 1977, vol. 55, pp. 2799-2806.
43. Agus, D. B., Gambhir, S. S., Pardridge, W. M., Spielholz, C., Baselga, J., Vera, J. C., and Golde, D. W. Vitamin C crosses the blood-brain barrier in the oxidized form through the glucose transporters. *Journal of Clinical Investigation*, 1997, vol. 100, pp. 2842.
44. Lin, Q., Li, Q., Batchelor-McAuley, C., and Compton, R. G. Two-Electron, Two-Proton Oxidation of Catechol: Kinetics and Apparent Catalysis. *The Journal of Physical Chemistry C*, 2015, vol. 119, pp. 1489-1495.
45. Runnels, P. L., Joseph, J. D., Logman, M. J., and Wightman, R. M. Effect of pH and surface functionalities on the cyclic voltammetric responses of carbon-fiber microelectrodes. *Analytical chemistry*, 1999, vol. 71, pp. 2782-2789.
46. Venton, B. J., Michael, D. J., and Wightman, R. M. Correlation of local changes in extracellular oxygen and pH that accompany dopaminergic terminal activity in the rat caudate–putamen. *Journal of neurochemistry*, 2003, vol. 84, pp. 373-381.
47. Lee, H., Dellatore, S. M., Miller, W. M., and Messersmith, P. B. Mussel-inspired surface chemistry for multifunctional coatings. *science*, 2007, vol. 318, pp. 426-430.
48. McCreery R. Advanced carbon electrode materials for molecular electrochemistry. *Chem. Rev*., 2008, vol. 108. pp. 2646-2687.
49. Patel, A. N., Tan, S. Y., Miller, T. S., Macpherson, J. V., and Unwin, P. R. Comparison and reappraisal of carbon electrodes for the voltammetric detection of dopamine. *Analytical chemistry*, 2013, vol. 85, pp. 11755-11764.
50. Ponchon, J. L., Cespuglio, R., Gonon, F., Jouvet, M., and Pujol, J. F. Normal pulse polarography with carbon fiber electrodes for in vitro and in vivo determination of catecholamines. *Analytical chemistry*, 1979, vol. 51, pp. 1483-1486.

51. Huffman, M. L., and Venton, B. J. Carbon-fiber microelectrodes for in vivo applications. *Analyst*, 2009, vol. 134, pp. 18-24.
52. Nebel, C. E., Rezek, B., Shin, D., Uetsuka, H., and Yang, N. Diamond for bio-sensor applications. *Journal of Physics D: Applied Physics*, 2007, vol. 40, pp. 6443.
53. Swain, G. M., and Ramesham, R. The electrochemical activity of boron-doped polycrystalline diamond thin film electrodes. *Analytical Chemistry*, 1993, vol. 65, pp. 345-351.
54. Kondo, T., Einaga, Y., Sarada, B. V., Rao, T. N., Tryk, D. A., and Fujishima, A. Homoepitaxial single-crystal boron-doped diamond electrodes for electroanalysis. *Journal of the Electrochemical Society*, 2002, vol. 149, pp. E179-E184.
55. Siew, P. S., Loh, K. P., Poh, W. C., and Zhang, H. Biosensing properties of nanocrystalline diamond film grown on polycrystalline diamond electrodes. *Diamond and related materials*, 2005, vol. 14, pp. 426-431.
56. Shalini, J., Lin, Y. C., Chang, T. H., Sankaran, K. J., Chen, H. C., Lin, I. N., Lee, C. Y., and Tai, N. H. Ultra-nanocrystalline diamond nanowires with enhanced electrochemical properties. *Electrochimica Acta*, 2013, vol. 92, pp. 9-19.
57. Robertson, J. Diamond-like amorphous carbon. Materials Science and Engineering: R: Reports, 2002, vol. 37, pp. 129-281.
58. Anders, A. (2009). Cathodic arcs: from fractal spots to energetic condensation, vol. 50. Springer Science & Business Media, 2009.
59. Grill, A. Diamond-like carbon coatings as biocompatible materials—an overview. *Diamond and related materials*, 2003, vol. 12, pp. 166-170.
60. Wisniewski, N., and Reichert, M. Methods for reducing biosensor membrane biofouling. *Colloids and Surfaces B: Biointerfaces*, 2000, vol. 18, pp. 197-219.
61. McCann, R., Roy, S. S., Papakonstantinou, P., Abbas, G., and McLaughlin, J. A. The effect of thickness and arc current on the structural properties of FCVA synthesised ta-C and ta-C: N films. *Diamond and related materials*, 2005, vol. 14, pp. 983-988.
62. Soin, N., Roy, S. S., Ray, S. C., Lemoine, P., Rahman, M. A., Maguire, P. D, Mitra, A. K. and McLaughlin, J. A. Thickness dependent electronic structure of ultra-thin

tetrahedral amorphous carbon (ta-C) films. *Thin Solid Films*, 2012, vol. 520, pp. 2909-2915.

63. Protopopova, V. S., Wester, N., Caro, M. A., Gabdullin, P. G., Palomäki, T., Laurila, T., and Koskinen, J. Ultrathin undoped tetrahedral amorphous carbon films: thickness dependence of the electronic structure and implications for their electrochemical behaviour. *Physical Chemistry Chemical Physics*, 2015, vol. 17, pp. 9020-9031.
64. Benlahsen, M., Cachet, H., Charvet, S., Debiemme-Chouvy, C., Deslouis, C., Lagrini, A., and Vivier, V. Improvement and characterization of the electrochemical reactivity of amorphous carbon nitride electrodes. *Electrochemistry communications*, 2005, vol. 7, pp. 496-499.
65. Li, W., Tan, C., Lowe, M. A., Abruna, H. D., and Ralph, D. C. Electrochemistry of individual monolayer graphene sheets. *ACS nano*, 2011, vol. 5, pp. 2264-2270.
66. Merkoçi, A., Pumera, M., Llopis, X., Pérez, B., del Valle, M., and Alegret, S. New materials for electrochemical sensing VI: carbon nanotubes. *TrAC Trends in Analytical Chemistry*, 2005, vol. 24, pp. 826-838.
67. Antolini, E. Carbon supports for low-temperature fuel cell catalysts. *Applied Catalysis B: Environmental*, 2009, vol. 88, pp. 1-24.
68. Sainio, S., Palomäki, T., Tujunen, N., Protopopova, V., Koehne, J., Kordas, K. Koskinen, J. Meyappan, M. and Laurila, T. Integrated Carbon Nanostructures for Detection of Neurotransmitters. *Molecular neurobiology*, 2015, vol. 52, pp. 859-866.
69. Prasek, J., Drbohlavova, J., Chomoucka, J., Hubalek, J., Jasek, O., Adam, V., and Kizek, R. Methods for carbon nanotubes synthesis—review. Journal of *Materials Chemistry*, 2011, vol. 21, pp. 15872-15884.
70. Grill, A. Diamond-like carbon: state of the art. *Diamond and related materials*, 1999, vol. 8, pp. 428-434.
71. Tanaka, Y., Furuta, M., Kuriyama, K., Kuwabara, R., Katsuki, Y., Kondo, T., Fujishima, A. and Honda, K. Electrochemical properties of N-doped hydrogenated amorphous carbon films fabricated by plasma-enhanced chemical vapor deposition methods. Electrochimica Acta, 2011, vol. 56, pp. 1172-1181.

72. Novoselov, K. S., Geim, A. K., Morozov, S. V., Jiang, D., Zhang, Y., Dubonos, S. A., Grigorieva, I.V and Firsov, A. A. Electric field effect in atomically thin carbon films. *science*, 2004, vol. 306, pp. 666-669.
73. Choi, W., Lahiri, I., Seelaboyina, R., and Kang, Y. S. Synthesis of graphene and its applications: a review. *Critical Reviews in Solid State and Materials Sciences*, 2010, vol. 35, pp. 52-71.
74. Pei, S., and Cheng, H. M. The reduction of graphene oxide. *Carbon*, 2012, vol. 50, pp. 3210-3228.
75. Zhu, Y., Murali, S., Cai, W., Li, X., Suk, J. W., Potts, J. R., and Ruoff, R. S. Graphene and graphene oxide: synthesis, properties, and applications. *Advanced materials*, 2010, vol. 22, pp. 3906-3924.
76. Hummers Jr, W. S., and Offeman, R. E. Preparation of graphitic oxide. *Journal of the American Chemical Society*, 1958, vol. 80, pp. 1339-1339.
77. Stankovich S., Dikin D. A., Piner R. D., Kohlhaas K. A., Kleinhammes A., Jia Y. Y., Wu, Y., Nguyen, S. T., and Ruoff, R. S., Synthesis of graphene-based nanosheets via chemical reduction of exfoliated graphite oxide. *Carbon,* 2007, vol. 45, pp. 1558–65.
78. Wang, G., Yang, J., Park, J., Gou, X., Wang, B., Liu, H., and Yao, J. Facile synthesis and characterization of graphene nanosheets. *The Journal of Physical Chemistry C*, 2008, vol. 112, pp. 8192-8195.
79. Si, Y., and Samulski, E. T. Synthesis of water soluble graphene. *Nano letters*, 2008, vol. 8, pp. 1679-1682.
80. Zhang, J., Yang, H., Shen, G., Cheng, P., Zhang, J., and Guo, S. Reduction of graphene oxide via L-ascorbic acid. *Chemical Communications*, 2010, vol. 46, pp. 1112-1114.
81. Chua, C. K., and Pumera, M. Chemical reduction of graphene oxide: a synthetic chemistry viewpoint. *Chemical Society Reviews*, 2014, vol. 43, pp. 291-312.
82. Shao, Y., Wang, J., Engelhard, M., Wang, C., and Lin, Y. Facile and controllable electrochemical reduction of graphene oxide and its applications. *Journal of Materials Chemistry*, 2010, vol. 20, pp. 743-748.

83. Peng, X. Y., Liu, X. X., Diamond, D., and Lau, K. T. Synthesis of electrochemically-reduced graphene oxide film with controllable size and thickness and its use in supercapacitor. *Carbon*, 2011, vol. 49, pp. 3488-3496.
84. Ferrari, A. C., and Robertson, J. Raman spectroscopy of amorphous, nanostructured, diamond–like carbon, and nanodiamond. *Philosophical Transactions of the Royal Society of London. Series A: Mathematical, Physical and Engineering Sciences*, 2004, vol. 362, pp. 2477-2512.
85. Liu, E., and Kwek, H. W. Electrochemical performance of diamond-like carbon thin films. *Thin Solid Films*, 2008, vol. 516, pp. 5201-5205.
86. Zhou, M., Wang, Y., Zhai, Y., Zhai, J., Ren, W., Wang, F., and Dong, S. Controlled Synthesis of Large-Area and Patterned Electrochemically Reduced Graphene Oxide Films. *Chemistry-A European Journal*, 2009, vol. 15, pp. 6116-6120.
87. Lounasvuori, M. M., Rosillo-Lopez, M., Salzmann, C. G., Caruana, D. J., and Holt, K. B. Electrochemical characterisation of graphene nanoflakes with functionalised edges. *Faraday discussions*, 2014, vol. 172, pp. 293-310.
88. Kachoosangi, R. T., and Compton, R. G. A simple electroanalytical methodology for the simultaneous determination of dopamine, serotonin and ascorbic acid using an unmodified edge plane pyrolytic graphite electrode. *Analytical and bioanalytical chemistry*, 2007, vol. 387, pp. 2793-2800.